EFFECTS OF THE In AND N DISTRIBUTION ON NANO-SCALE STRUCTURES IN NEARLY LATTICE-MATCHED InGaPN ON GaAs (001) GROWN BY MOVPE

Mr. Phongbandhu Sritonwong

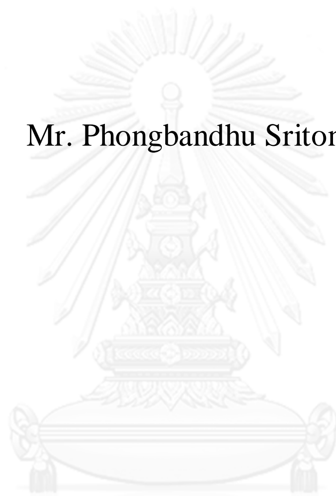

บทคัดย่อและแฟ้มข้อมูลฉบับเต็มของวิทยานิพนธ์ตั้งแต่ปีการศึกษา 2554 ที่ให้บริการในคลังปัญญาจุฬาฯ (CUIR)
เป็นแฟ้มข้อมูลของนิสิตเจ้าของวิทยานิพนธ์ ที่ส่งผ่านทางบัณฑิตวิทยาลัย
The abstract and full text of theses from the academic year 2011 in Chulalongkorn University Intellectual Repository (CUIR)
are the thesis authors' files submitted through the University Graduate School.

A Dissertation Submitted in Partial Fulfillment of the Requirements
for the Degree of Doctor of Philosophy Program in Nanoscience and Technology
(Interdisciplinary Program)
Graduate School
Chulalongkorn University
Academic Year 2015
Copyright of Chulalongkorn University

อิทธิพลของการกระจายตัวของ In และ N ที่มีต่อ InGaPN บน GaAs (001) ที่มีโครงผลึกเกือบตรงกัน ปลูกโดยเอ็มโอวีพีอี

นายพงษ์พันธุ์ ศรีต้นวงศ์

วิทยานิพนธ์นี้เป็นส่วนหนึ่งของการศึกษาตามหลักสูตรปริญญาวิทยาศาสตรดุษฎีบัณฑิต
สาขาวิชาวิทยาศาสตร์นาโนและเทคโนโลยี (สหสาขาวิชา)
บัณฑิตวิทยาลัย จุฬาลงกรณ์มหาวิทยาลัย
ปีการศึกษา 2558

ลิขสิทธิ์ของจุฬาลงกรณ์มหาวิทยาลัย

Thesis Title	EFFECTS OF THE In AND N DISTRIBUTION ON NANO-SCALE STRUCTURES IN NEARLY LATTICE-MATCHED InGaPN ON GaAs (001) GROWN BY MOVPE
By	Mr. Phongbandhu Sritonwong
Field of Study	Nanoscience and Technology
Thesis Advisor	Assistant Professor Sakuntam Sanorpim, Ph.D.

Accepted by the Graduate School, Chulalongkorn University in Partial Fulfillment of the Requirements for the Doctoral Degree

.... Dean of the Graduate School
(Associate Professor Sunait Chutintaranond, Ph.D.)

THESIS COMMITTEE

.... Chairman
(Associate Professor Vudhichai Parasuk, Ph.D.)

.... Thesis Advisor
(Assistant Professor Sakuntam Sanorpim, Ph.D.)

.... Examiner
(Assistant Professor Sukkaneste Tungasmita, Ph.D.)

.... Examiner
(Ratthapol Rangkupan, Ph.D.)

.... External Examiner
(Kittipong Tantisantisom, Ph.D.)

พงษ์พันธุ์ ศรีต้นวงศ์ : อิทธิพลของการกระจายตัวของ In และ N ที่มีต่อ InGaPN บน GaAs (001)ที่มีโครงผลึกเกือบตรงกัน ปลูกโดยเอ็มโอวีพีอี (EFFECTS OF THE In AND N DISTRIBUTION ON NANO-SCALE STRUCTURES IN NEARLY LATTICE-MATCHED InGaPN ON GaAs (001) GROWN BY MOVPE) อ.ที่ปรึกษาวิทยานิพนธ์หลัก: ผศ. ดร. สกุลธรรม เสนาะพิมพ์, 71 หน้า.

วิทยานิพนธ์นี้รายงานผลของการเติมไนโตรเจน (N) ต่อการกระจายตัวของโลหะผสม (alloy fluctuation) ความเป็นระเบียบเชิงโครงสร้าง (structural ordering) และการรวมตัวแบบไม่เปล่งแสง (non-radiative recombination) ในฟิล์มอินเดียมแกลเลียมฟอสไฟไนไตร์ (InGaPN) บนวัสดุฐานรองแกลเลียมอาเซไนส์ (GaAs) ผิวระนาบ (001) ฟิล์มอินเดียมแกลเลียมฟอสไฟไนไตร์เตรียมโดยวิธี เมทัลออร์แกนิกเวเปอร์เฟสอิพิแทกซี่ (Metal Organic Vapor Phase Epitaxy, MOVPE) โดยมีอัตราการไหลของไดเมทิลไฮดราซีน (Dimethyl Hydrazine, DMHy) อยู่ในช่วง 0 ถึง 1,100 ไมโครโมลต่อนาที นอกจากนี้ ฟิล์ม InGaPN ได้ถูกนำไปอบด้วยความร้อนด้วยกระบวนการอบความร้อนแบบฉับพลัน (Rapid Thermal Annealing, RTA) ปริมาณสารอินเดียม (In) และ N ในฟิล์ม InGaPN ถูกตรวจสอบด้วยเทคนิคการผสมผสานผลที่ได้จากการเลี้ยวเบนรังสีเอกซ์กำลังแยกสูง (High Resolution X-ray Diffraction, HRXRD) และการกระเจิงแบบรามาน (Raman scattering) จากผลการตรวจวัดด้วยการกระเจิงแบบรามานได้ปริมาณ In เป็น 56.4±0.8%, 55.8±0.8%, 55.9±0.9% และ 55.7±1.1% เมื่ออัตราการไหลของ DMHy เพิ่มจาก 0, 300, 700 และ 1,100 ไมโครโมลต่อนาที ตามลำดับ ในทางเดียวกันปริมาณ N ก็เพิ่มจาก 0, 0.9±0.4%,1.4±0.4% และ 2.1±0.5% ตามลำดับ ผลจากการตรวจวัดเทคนิคการกระเจิงแบบรามาน พบว่าความเป็นระเบียบเชิงโครงสร้างในระดับที่มีผลกระทบต่อค่าช่องว่างแถบพลังงานน้อยมากจนหรือจนถึงระดับไม่มีผลกระทบ นอกจากนี้ยังพบการลดลงของความเข้มของการเปล่งแสงรวม ซึ่งชี้ให้เห็นถึงการเพิ่มขึ้นของการรวมตัวแบบไม่เปล่งแสง พร้อม ๆ กันกับปริมาณ N ที่เพิ่มขึ้น ผลของ RTA แสดงการเพิ่มขึ้นของของความเข้มของการเปล่งแสงรวม ซึ่งเป็นตัวบ่งชี้สำคัญของการลดลงของการรวมตัวแบบไม่เปล่งแสง นอกจากนี้ยังพบการเพิ่มขึ้นของปริมาณ N ซึ่งเหนี่ยวนำให้ความเป็นระเบียบเชิงโครงสร้างเพิ่มขึ้นอีกด้วย ยิ่งไปกว่านั้น กระบวนการ RTAได้ปรับปรุงคุณภาพผลึกโดยเพิ่มความสม่ำเสมอในการกระจายตัวของโลหะผสมในฟิล์ม InGaPN เนื่องด้วยผลจากการจัดเรียงตัวของอะตอมในโครงสร้างใหม่ ฟิล์ม InGaPN ที่มีคุณภาพผลึกดีที่สุดนั้น มีความแตกต่างโครงผลึกกับ GaAs เพียงร้อยละ 0.12 เป็นฟิล์มที่ปลูกด้วยอัตราการไหลของ DMHy เท่ากับ 1,100 ไมโครโมลต่อนาทีและเวลาในการทำ RTA ที่ 120 วินาที

สาขาวิชา วิทยาศาสตร์นาโนและเทคโนโลยี ลายมือชื่อนิสิต ....

ปีการศึกษา 2558 ลายมือชื่อ อ.ที่ปรึกษาหลัก ....

5487842220 : MAJOR NANOSCIENCE AND TECHNOLOGY

KEYWORDS: INGAPN / MOVPE / ANNEALING / ORDERING EFFECT

PHONGBANDHU SRITONWONG: EFFECTS OF THE In AND N DISTRIBUTION ON NANO-SCALE STRUCTURES IN NEARLY LATTICE-MATCHED InGaPN ON GaAs (001) GROWN BY MOVPE. ADVISOR: ASST. PROF. SAKUNTAM SANORPIM, Ph.D., 71 pp.

Abstract

In the dissertation, an effect on N incorporation on alloy fluctuation, structural ordering and non-radiative recombination in the InGaPN films on GaAs (001) substrates are systematically investigated. All the InGaPN films were grown by metalorganic vapor phase epitaxy (MOVPE) with different DMHy flow rates of 0, 300, 700 and 1,100 mmol/min. To improve crystal quality, the InGaPN films were thermally annealed using rapid thermal annealing (RTA) process, which was performed at 650 ^{O}C for 30, 60, 120 and 180 seconds under N_2 ambient. To examine the In and N contents, a combination of HRXRD and Raman spectroscopy measurements has been applied for the nearly lattice-matched InGaPN films grown on GaAs (001) substrates. The structural ordering was measured by the Raman spectroscopy and the non-radiative recombination center are studied by room temperature photoluminescence (PL) spectroscopy. According to Raman scattering results, the In content, which is slightly effected by an introduction DMHy during the growth, was determined to be 56.4±0.8 at%, 55.8±0.8 at%, 55.9±0.9 at% and 55.7±1.1 at% with increasing DHMy flow rates from 0 to 1,100 μmol/min. Consequently, the N content was determined to be 0, 0.9±0.4 at%,1.4±0.4 at% and 2.1±0.5% with increasing DHMy flow rates. Raman spectroscopy results show a weak structural ordering to be the level that no effect on an optical bandgap. Decreasing of an integrate intensity of PL spectra with increasing of the N content indicates an increase of the non-radiative recombination centers. After RTA process, PL spectra exhibited higher intensity. This indicates a reduction of the non-radiative recombination centers. The InGaPN samples were annealed at 650 ^{O}C at 30, 60, 120 and 180 seconds. Further, HRXRD results show a reduction of alloy fluctuation due to crystal reorganization mechanism. The increasing of N content, which results in an increase of structural ordering, was observed after RTA. The best film quality with lowest misfit strain of 0.12% was obtained for the InGaPN film grown with DMHy flow rate of 1,100 μmol/min and annealing time of 120 s.

Field of Study: Nanoscience and Technology Student's Signature ....

Academic Year: 2015 Advisor's Signature ....

ACKNOWLEDGEMENTS

I would like to fully appreciate my advisor, Assistance Professor Dr. Sakuntam Sanorpim for his valuable suggestion and work hard for supporting me everything in this thesis. He always gives me a good attention and valuable experience during my PhD study.

I would like to acknowledge my thesis committee Associate Professor Dr. Vudhichi Parasuk, Assistant Professor Dr. Sukaneste Tungasamita, Dr. Ratthapol Rangupan and Dr. Kittipong Tantisantisom for their comment on this thesis.

Special thanks to Mrs. Nasuangsorn Yopanaksakdi, Program coordinator in Nanoscience and Technology for helping me in academic document during the study in this program.

I would like to thank my colleagues from AMPRG member. Mrs. Pawinee Klangtakai, Ms. Dares Kaewket, Ms. Pornsiri Wanarattikarn, Mr. Pattana Suwanyangyaun, Mr. Taworn Intaro, Ms Jamroenta Parinyataramas, Ms. Papaporn Jantawongrit, and Mr. Noppadon Toongyai for his helpful in discussion and joyful time.

Thanks Graduate school, Chulalongkorn University, Rajabhat Undornthani University, The Ratchadapiseksomphot Endowment Fund of Chulalonkorn University (RES560530229-EN) and The 90th Anniversary of Chulalongkorn University Fund (Ratchadapiseksomphot Endowment Fund) for financials support.

Last but not least, I really deeply thanks to my family, my father in heaven, my mother in my heart and my kind brother and his wife for their love, understand and support for this long journey.

CONTENTS

Page

THAI ABSTRACT ... iv
ENGLISH ABSTRACT ... v
ACKNOWLEDGEMENTS ... vi
CONTENTS ... vii
CHAPTER I INTRODUCTIONS ... 1
1.1 Overview and Motivation of InGaPN ... 1
1.2 Objective and Scope of the Dissertation ... 6
1.3 Organization of the Dissertation ... 7
CHAPTER II InGaPN BACKGROUND ... 8
2.1 InGaPN Alloys Semiconductors ... 8
2.1.1 Misfit-Strain and Composition of InGaPN Epilayer ... 8
2.1.2 Optical Properties of InGaPN ... 12
2.2 Solar Cell Application ... 13
2.2.1 Multijunction Solar Cells ... 13
2.3 Ordering Effects ... 14
CHAPTER III GROWTH AND ANALYTICAL METHODS ... 18
3.1 Metal Organic Chemical Vapor Phase Deposition (MOCVD) ... 18
3.1.1 Growth of Samples ... 19
3.2 Characterized Methods ... 20
3.2.1 High Resolution X-ray Diffraction ... 20
3.2.2 Raman Scattering ... 23
3.2.3 Photoluminescence ... 25
CHAPTER IV RESULTS AND DISCUSSIONS ... 26
4.1 Alloy Composition Investigations of Nearly Lattice-Matched InGaPN Films ... 26
4.2 Effect of N Incorporation on Alloy Fluctuation, Ordering Effect and Non-radiative Recombination Center in InGaPN on GaAs Substrate ... 35
4.2.1 Surface Morphology and Alloy Fluctuation ... 35
4.2.3 Non-radiative Recombination Center ... 41

Chulalongkorn University

Page

4.3 Effects of Rapid Thermal Annealing on Alloy Fluctuation, Ordering Effect and Non-radiative Recombination Center of InGaPN on GaAs 44
4.3.1 Surface Morphology and Alloy Fluctuation after RTA.......................... 44
4.3.2 Alloy Composition after RTA... 49
4.3.3 Non-radiative Recombination Center after RTA 58
4.3.4 Ordering Effect on N Contents after RTA 61
CHAPTER V CONCLUSIONS.. 63
REFERENCES.. 66
APPENDIX... 68
APPENDIX A 69
VITA... 71

จุฬาลงกรณ์มหาวิทยาลัย
Chulalongkorn University

LIST OF TABLES

Table 2-1 Relaxed lattice constant (a_0) and elastic constants (C_{11} and C_{12}) of GaP , cubic-GaN , InP and cubic-InN . C_{11} and C_{12} are in unit of 10^{11} dyn/cm^2. 12

Table 4-1 Relaxed lattice constant (a_o), misfit strain (ε ||) and In content determined by micro-Raman spectroscopy) and calculated N content. Noted that the In content determined by HRXRD is 56.6±1.7 at%. 34

Table 4-2 b/a ratio, ordering parameter (η), band-gap energy (E_g) and $\Delta E_{g(\eta=1)}\eta^2$ of InGaP(N)... 39

Table 4-3 show the band-gap energy, FWHM and the integrate intensity ratio of an InGaPN on InGaP 42

Table 4-4 Relaxed lattice constant (a_o), misfit strain (ε ||) and In content determined by micro-Raman spectroscopy) and calculated N content of DMHy 300 μmol/min. 55

Table 4-5 Relaxed lattice constant (a_o), misfit strain (ε ||) and In content determined by micro-Raman spectroscopy) and calculated N content of DMHy 700 μmol/min. 55

Table 4-6 Relaxed lattice constant (a_o), misfit strain (ε ||) and In content determined by micro-Raman spectroscopy) and calculated N content of DMHy 1,100 μmol/min. 55

Table 4-7 show the band-gap energy of the annealing InGaPN with vary DMHy 300, 700 and 1,100 μmol/min 59

Table 4-8 show the b/a ratio of the annealing InGaPN with vary DMHy 300, 700 and 1,100 μmol/min.. 61

LIST OF FIGURES

Fig. 1-1 The bandgap energy as a function of lattice constant for III-V compound semiconductors 2

Fig. 1-2 The InGaP/GaAs/InGaAsN/Ge four-junction-structure solar cells. 3

Fig. 1-3 Plot of record solar cell efficiencies for different technologies, showing the high efficiency for III-V multijunction solar cells 5

Fig. 1-4 Schematic of the InGaPN CuPt-B structure. 6

Fig. 2-1 Schematic illustration of (a) latticed-matched, (b) coherently strained lattice-matched and (c) relaxed latticed-matched epitaxy. 9

Fig. 2-2 Schematic diagram of Bragg's law. 10

Fig. 2-3 Schematic drawing shows the light absorption of multijunction solar cell... 13

Fig. 2-4 InGaPN structure, Zincblende structure (Left) and CuPt-B structure (Right). 14

Fig. 2-5 The definitions of a and b from the InGaPN/GaAs Raman scattering. 17

Fig. 3-1 Schematic of growth process of InGaPN. 19

Fig. 3-2 Schematic of the High Resolution X-ray diffraction (HRXRD). 21

Fig. 3-3 Bruker AXS D8 Discovery HRXRD machine at at research institute, Chulalongkorn university. 23

Fig. 3-4 Schematic of Raman scattering measurement with back scattering geometry. 24

Fig. 4-1 HRXRD $2\theta/\omega$ profiles of (a) InGaP film and (b) – (d) InGaPN films grown on GaAs (001) substrates as dependent on DMHy flow rates. 27

Fig. 4-2 HRXRD 2θ/ω and Δω reciprocal space maps around an asymmetrical (115) reflection for the InGaPN films on GaAs (001) substrates as dependent on the DMHy flow rates, (a) 0, (b) 300, (c) 700 and (d) 1,100 μmol/min. 29

Fig. 4-3 Raman spectra of InGaPN films grown on GaAs (001) substrates with various DMHy flow rates of (a) 0, (b) 300, (c) 700 and (d) 1,100 μmol/min. 30

Fig. 4-4 The In and N content of the InGaPN films as dependent DMHy flow rates grown with [TMIn]/([TMIn]+[TMGa]) ratio of 0.63 33

Fig. 4-5 show the surface morphology of the InGaP(N) alloy films which observed by atomic force microscopy (AFM) with a scanning area of 10x10 μm^2 of DMHy (a) 0 (b) 300, (c) 700 and (d) 1,100 μmol/min. 36

Fig. 4-6 show the surface morphology of the InGaP(N) alloy films which observed by scanning electron microscope (SEM) with a scanning of DMHy (a) 0 (b) 300, (c) 700 and (d) 1,100 μmol/min. 37

Fig. 4-7 show cross-sectional SEM images of the corresponding InGaPN film with thickness of DMHy (a) 0, (b) 300, (c) 700 and (d) 1,100 μmol/min. 37

Fig. 4-8 Raman spectra of (a) N-free InGaP and InGaPN films grown on GaAs (001) substrates with various N contents (b) 0.9%, (c) 1.4% and (d) 2.1%. 38

Fig. 4-9 b/a ratio and band-gap energy as the function of N contents of N-free InGaP and InGaPN with various N contents 0.9%, 1.4% and 2.1%. 40

Fig. 4-10 a room-temperature PL of (a) N-free InGaP and InGaPN with various N contents (b) 0.9%, (c) 1.4% and (d) 2.1%.. 43

Fig. 4-11 band-gap energy of (●) N-free InGaP and InGaPN with various N contents (■) 0.9%, (▲) 1.4% and (♦) 2.1%. 43

Fig. 4-12 show surface RMS as the annealing time function of InGaPN. 45

Fig. 4-13 AFM images of the $In_xGa_{1-x}P_{1-y}N_y$ alloys films with DMHy 300 μmol/min grown on the GaAs (001) substrates rapid thermal annealing at annealing temperature 650 ^{O}C with varied the annealing times. 46

Fig. 4-14 AFM images of the $In_xGa_{1-x}P_{1-y}N_y$ alloys films with DMHy 700 μmol/min grown on the GaAs (001) substrates rapid thermal annealing at annealing temperature 650 ^{O}C with varied the annealing times. 47

Fig. 4-15 AFM images of the $In_xGa_{1-x}P_{1-y}N_y$ alloys films with DMHy 1,100 μmol/min grown on the GaAs (001) substrates rapid thermal annealing at annealing temperature 650 ^{O}C with varied the annealing times. 48

Fig. 4-16 HRXRD (004) $2\theta/\omega$ curves of $In_xGa_{1-x}P_{1-y}N_y$ alloys films grown on GaAs (001) substrates with varied the DMHy flow rate (a) 300, (b) 700 and (c) 1,100 μmol/min at different annealing time 0 – 180 s. at annealing temperature 650 ^{O}C. 49

Fig. 4-17 HRXRD 2θ/ω and Δω reciprocal space maps around an asymmetrical (115) reflection for the InGaPN films on GaAs (001) on the DMHy flow rates 300 μmol/min with annealing time (a) as grown, (b) 30, (c) 60, (d) 120 and (e) 180 s at 650 ^{O}C. 51

Fig. 4-18 HRXRD 2θ/ω and Δω reciprocal space maps around an asymmetrical (115) reflection for the InGaPN films on GaAs (001) on the DMHy flow rates 700 μmol/min with annealing time (a) as grown, (b) 30, (c) 60, (d) 120 and (e) 180 s at 650 ^{O}C. 52

Fig. 4-19 HRXRD 2θ/ω and Δω reciprocal space maps around an asymmetrical (115) reflection for the InGaPN films on GaAs (001) on the DMHy flow rates 1,100 μmol/min with annealing time (a) as grown, (b) 30, (c) 60, (d) 120 and (e) 180 s at 650 ^{O}C. 53

Fig. 4-20 illustrate Raman spectra of the InGaPN alloy films with different DMHy flow rates of (a) 300, (b) 700 and (c) 1,100 μmol/min, respectively. The different annealing time were applied to as grown and annealed InGaPN at 30, 60, 120, and 180 s. for each DHMy flow rates. 54

Fig. 4-21 In and N content as the function annealing time of (●) DMHy 300 μmol/min, (■) DMHy 700 μmol/min and (♦) 1,100 μmol/min. 57

Fig. 4-22 a room-temperature PL of (a) annealing InGaPN with various DMHy flow rates and N contents as the function of the annealing times. 59

Fig. 4-23 a room-temperature PL of (a) annealing InGaPN with various DMHy flow rates (a) 300, (b) 700 and (c) 1,100 μmol/min. The annealing time is 0 (as grown), 30, 60, 120 and 180 s. as label in the graph. 60

Fig. 4-24 show the b/a ratio and N content as the function of annealing time of InGaPN with different DMHy flow rate. 62

จุฬาลงกรณ์มหาวิทยาลัย
Chulalongkorn University

CHAPTER I
INTRODUCTIONS

1.1 Overview and Motivation of InGaPN

A quaternary alloy InGaPN semiconductor is a novel material which is extensive studied due to its unique physical properties. For the InGaPN alloy, the lattice constant can be adjusted by controlling the composition of nitrogen (N) and indium (In) to lattice-matched with various substrates, such as GaAs [1, 2] and GaP [3]. When Ga atom is replaced by In atom, the lattice constant of the alloy will be increased due to a larger size of In atom compare to Ga atom. Otherwise, adding a smaller N atom to replace the bigger phosphorus (P) atom sized result in a decreasing of the lattice constant. The InGaPN has the huge bowing parameter, which an adding a few

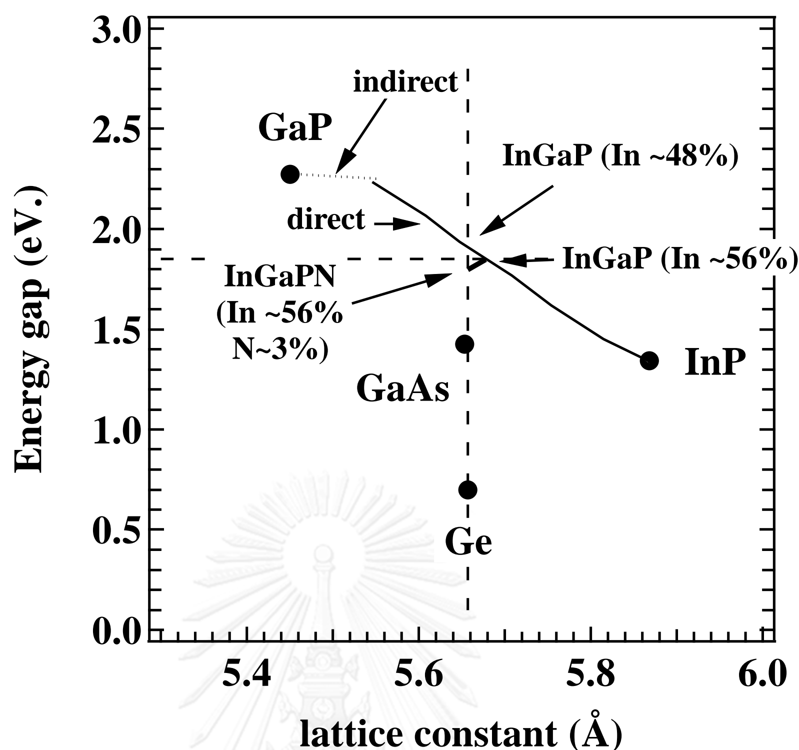

Fig. 1-1 The bandgap energy as a function of lattice constant for III-V compound semiconductors

จุฬาลงกรณ์มหาวิทยาลัย
Chulalongkorn University

percentage of N can cause a large reduction of its bandgap energy [3, 4]. Fig. 1-1 showed the bandgap energy as a function of lattice constant for InGaPN compound semiconductor. Thus, both its lattice constant and bandgap energy can be adjusting by the alloy composition (In and N) made it has a potential to may applications such as light emitting diode (LEDs), laser diodes (LDs) [1, 5, 6], heterojunction bipolar transistors and especially solar cells [1, 2].

In solar cells application as mention above, in order to reach high efficiency of solar conversion, the multijunction solar cell are developed which the solar spectrum has to be subdivided and converted by different absorber layers with optimized bandgap. The high bandgap energy at top cell layer converses the short wavelength fraction and permits the long-wavelength to convert at a lower cell in the stack. This is

called high-efficiency multijunction solar cells. The divide of the layer of this solar cells are expected that more number of p-n junctions will be reduced a less thermalization and transmission losses in the solar cell resulting in higher efficiency. Four-junction solar cell, one of the example of multijunction solar cells, as shown in Fig. 1-2. At the bottom absorber layer, germanium (Ge) is use to absorb in the energy length 0.67 to 1.00 eV, the second layer is InGaAsN for 1.00 to 1.40 eV, InGaAs is the third layer for absorbed 1.40 to 1.80 eV and the top layer the InGaPN is used to absorbed the energy from 1.85 eV and above. Recently, Fig. 1-3, the highest efficiency is recorded at about 40% for III-V semiconductors (InGaP/GaAs/Ge) multijunction solar cell under concentrated sunlight [7]. From the quantum efficiency (QE) analyzing, semiconductor materials with 1.8-2.3 eV bandgap energy [8], which are a member of III-V semiconductors, are suitable to be an absorber layer on GaAs based high efficiency multi-junction solar cells. InGaPN is a promising candidate because its optical bandgap can be modified in this range, ~1.4 to ~2.2 eV, as shown in Fig. 1-1. One of successive

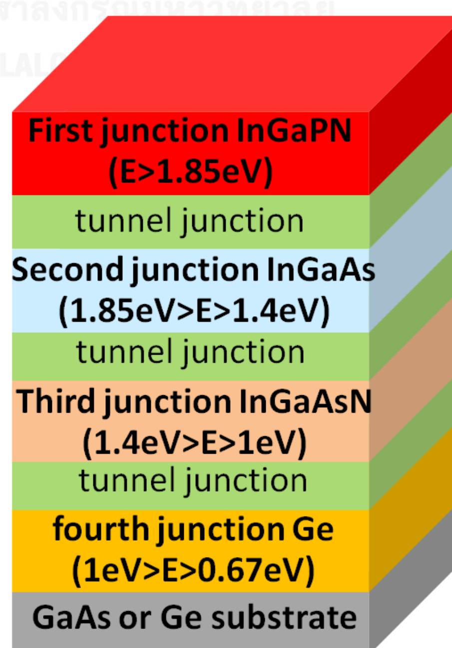

Fig. 1-2 The InGaP/GaAs/InGaAsN/Ge four-junction-structure solar cells.

way to approach the maximum efficiency is the variety of semiconductors with different bandgaps and lattice-match conditions. This is a challenge for the use of quaternary III-III-V-N semiconductors such as InGaPN as the absorber layer in multijunction solar cells. The other interesting properties of III- V alloyed is the variation of its optical bandgap from the structure orientation, “ordering effect”, such as InGaP, AlGaAs, InGaPAs and InGaPN [9, 10], The optical bandgap will be varying from 1.85 eV for an “ordered” structure to 2.00 eV for a “disordered” (i.e. random alloy) $In_{0.48}Ga_{0.52}P$ structure [11]. The “ordering effect” is reported by the formation of different atomic structure (i.e. Cu–Pt or Td structure in ordered and disordered material, respectively). In Cu–Pt structure, Fig. 1-4, the group-III sublattice (In and Ga) exhibits a super-lattice structure in the $[111]_B$ direction. It causes a reduction in the bandgap energy and splitting of the valence band which can affect the electronic and optical properties of the material [12, 13]. To control the bandgap energy of InGaPN suited for the top absorption layer of multijunction solar cells, the ordering effect properties of InGaPN will be studied to reduce the parameter of the variation of bandgap energy in InGaPN.

Chulalongkorn University

To improve of the optical and structural properties of InGaPN, the post-growth rapid thermal annealing is applied. RTA process is usually performing on ternary InGaP and InGaPN quaternary alloys to improve non-radiative defect and to enhance their luminescence intensity.

Fig. 1-3 Plot of record solar cell efficiencies for different technologies, showing the high efficiency for III-V multijunction solar cells.

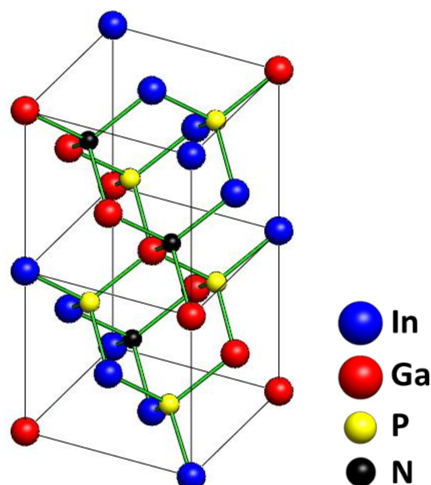

Fig. 1-4 Schematic of the InGaPN CuPt-B structure.

จุฬาลงกรณ์มหาวิทยาลัย
Chulalongkorn University

1.2 Objective and Scope of the Dissertation

The purpose of this work is to establish a basic understanding of structural and optical properties of InGaPN alloy films with very N incorporation for developing the efficiency of the top layer of multijunction solar cell. The following topics are mainly focus

i) Effects of the N incorporation on the structural and optical properties of InGaPN alloy films

ii) Annealing effects on the structural and optical properties of InGaPN alloy films

In order to verify the InGaPN material both structural and optical properties, high resolution X-ray diffraction (HRXRD) and Raman scattering have been used for a tools to determine the alloy compositions and crystal quality and especially the atom ordering in the InGaPN alloy films. Photoluminescence used for determined the

bandgap energy. Which is believed that the information obtained from this dissertation can be fulfill the knowledge for fabrication of the InGaPN base high-efficiency III-III-V -nitride solar cells.

1.3 Organization of the Dissertation

The organized of this dissertation is following by:

In chapter I, the overview and motivation of InGaPN semiconductor, challenge and applications were described.

In chapter II, The Background of InGaPN are described which consisted of Alloy composition, solar cell application, and the ordering effect.

In chapter III, growth and analytical method which can be describe in term evaluation of strain and composition, observation of bandgap and vibration property by using High Resolution X-ray diffraction (HRXRD), Photoluminescence and Raman spectroscopy, respectively.

In chapter IV, results and discussion are divide into three part, first strain and composition, follow by the structural and optical properties change by N incorporation and the last is the annealing effect on structural and optical properties of InGaPN alloy.

Finally, In chapter V, conclusion of this dissertation

CHAPTER II
InGaPN BACKGROUND

2.1 InGaPN Alloys Semiconductors

จุฬาลงกรณ์มหาวิทยาลัย
CHULALONGKORN UNIVERSITY

The tunable of the lattice constant and bandgap of energy of InGaPN alloys make this alloys is potential to may applications such as light emitting diode (LEDs), laser diodes (LDs), heterojunction bipolar transistors and solar cells. Both its lattice constant and bandgap energy can be adjusting by the alloy composition (In and N). The different in composition of the alloy can cause vary strained on the alloy layers.

2.1.1 Misfit-Strain and Composition of InGaPN Epilayer

When the epilayer was grow on the substrate layer. There are three essential concept of strained-layer as shown on Figure 2-1. In Fig. 2-1 (a) an epilayer is grown on a same crystal structure and lattice parameter substrate. In Fig. 2-1 (b) an epilayer is

grown on a different lattice parameter substrate and an epilayer is grown on a different lattice parameter substrate with a certain layer thickness, or critical thickness, the epilayer become enthusiastically favorable to reduce the elastic strain by introduce a misfit dislocation as illustrate in Fig. 2-1 (c).

Assuming enough symmetry, the misfit strain is given by

$$\varepsilon = \frac{a_{epi}}{a_s} - 1 \qquad (2\text{-}1)$$

Where a_{epi} and a_s are the free lattice parameters of the epilayer and the substrate layer, respectively. If the epilayer is partially relaxed, the strain parallel $(\varepsilon_{\parallel})$ and perpendicular $(\varepsilon_{\perp})$ to the substrate can be evaluate by the expressions

$$\varepsilon_{\parallel} = \frac{a_{\parallel}}{a_s} - 1 \qquad (2\text{-}2)$$

and

$$\varepsilon_{\perp} = \frac{a_{\perp}}{a_s} - 1 \qquad (2\text{-}3)$$

จุฬาลงกรณ์มหาวิทยาลัย

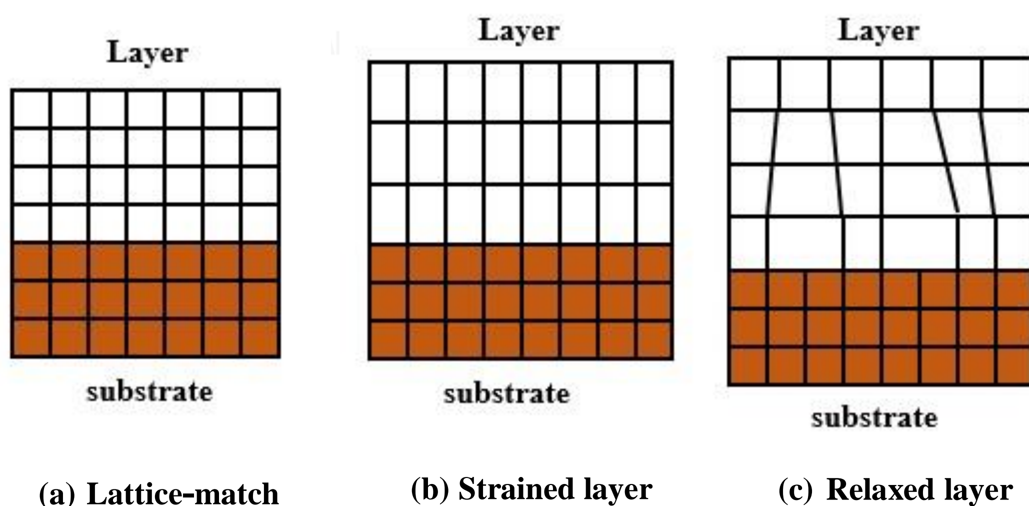

Fig. 2-1 Schematic illustration of (a) latticed-matched, (b) coherently strained lattice-matched and (c) relaxed latticed-matched epitaxy.

The alloy composition can be determined by using the interpolation method. For the $In_xGa_{1-x}P$ ternary alloys, the lattice constant (a) can be linearly interpolated by

$$a_{InGaP} = x.a_{InP} + (1-x).a_{GaP} \quad (2\text{-}4)$$

Which x is the In content.

Then for the quaternary alloy, the equation 2-4, will be modified to

$$a_{InGaPN} = (1-x)[(1-y)a_{GaP} + ya_{GaN}] + x[(1-y)a_{InP} + ya_{InN}] \quad (2\text{-}5)$$

Which x is the In content and y is the N contents.

To obtained the lattice constant of InGaPN films in perpendicular ($a_{\perp}$) a symmetric reflection in (004) planes were measure by HRXRD 2θ/ω mode, according to Bragg's Law

$$2dsin\theta = n\lambda \quad (2\text{-}6)$$

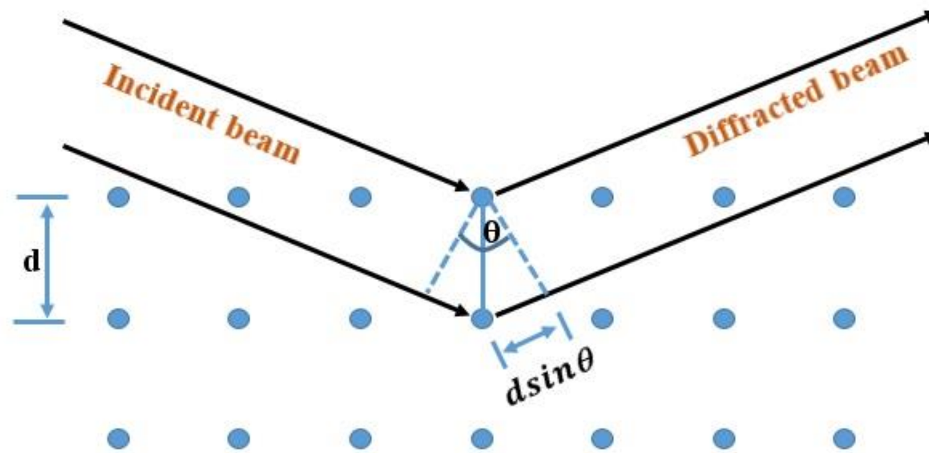

Fig. 2-2 Schematic diagram of Bragg's law.

By describe in Fig 2-2, θ is the angle between the direction of an incident beam and a corresponding investigated plane or Bragg's angle. From HRXRD measurement, Bragg's angle (θ) and wavelength (λ) can be obtained. Due to the InGaPN structure is a tetragonal structure and their lattice parameter can be obtained by

$$\frac{1}{d^2} = \frac{h^2}{a_{\parallel}^2} + \frac{k^2}{a_{\parallel}^2} + \frac{l^2}{a_{\perp}^2} \tag{2-7}$$

The parallel lattice parameter ($a_{\parallel}$) can be obtained by an asymmetric reflection in (115) planes were measure by HRXED Δω-scan mode. The inclination between the (115) planes of the substrate and the layer of the specimens can be detect owing to tetragonal distortion. Then the angle between the (115) plane and (001) plane (ω) of the InGaPN layer differs from the GaAs substrate. Thus, tilt angle (Δω) is given by

$$\Delta\omega = \omega_1 - \omega_2 = tan^{-1}\left(\frac{\sqrt{2}}{5}\right) - tan^{-1}\left(\frac{\sqrt{2}a_{\parallel}}{5a_{\perp}}\right) \tag{2-8}$$

This Δω equation is satisfied by assuming that the GaAs substrate is fully strain. By the combination of 2θ/ω mode ($a_{\perp}$) and Δω equation, $a_{\parallel}$ can be determined. Thus, the lattice constant (a), N and in content were determined by the set of these equation

$$a_{InGaPN} = \frac{2.C_{12}.a_{//} + C_{12}.a_{\perp}}{2.C_{12} + C_{11}} \tag{2-9}$$

$$a_{InGaPN} = (1-x)[(1-y)a_{GaP} + ya_{GaN}] + x[(1-y)a_{InP} + ya_{InN}] \tag{2-10}$$

$$C_{11} = \frac{(1-x)[(1-y)a_{GaP}C_{11}^{GaP} + ya_{GaN}C_{11}^{GaN}}{a_{InGaPN}} + \frac{x[(1-y)a_{InP}C_{11}^{InP} + ya_{InN}C_{11}^{InN}]}{a_{InGaPN}} \tag{2-11}$$

$$C_{12} = \frac{(1-x)[(1-y)a_{GaP}C_{12}^{GaP} + ya_{GaN}C_{12}^{GaN}}{a_{InGaPN}} + \frac{x[(1-y)a_{InP}C_{12}^{InP} + ya_{InN}C_{12}^{InN}]}{a_{InGaPN}} \tag{2-12}$$

Table 2-1 Relaxed lattice constant (a_o) and elastic constants (C_{11} and C_{12}) of GaP , cubic-GaN , InP and cubic-InN . C_{11} and C_{12} are in unit of 10^{11} dyn/cm^2.

Parameters	GaP	Cubic-GaN	InP	Cubic-InN
a_o (Å)	5.450[14]	4.503[15]	5.868[16]	4.98[15]
C_{11}	14.12[17]	26.4[15]	10.22[18]	17.2[19]
C_{12}	6.253[17]	15.3[15]	5.76[18]	11.9[19]

Where C_{11} and C_{12} are the elastic constants for $In_xGa_{1-x}P_{1-y}N_y$, and a_{GaP}, a_{GaN}, a_{InP} and a_{InN} are the equilibrium lattice constants of GaP, cubic-GaN, InP and cubic-InN, respectively. Since the elastic constants of $In_xGa_{1-x}P_{1-y}N_y$ are not available, they can, thus, be derived from the elastic constants of the four binary compounds by using the interpolation scheme.

จุฬาลงกรณ์มหาวิทยาลัย
Chulalongkorn University

2.1.2 Optical Properties of InGaPN

The quaternary InGaPN alloy show a huge bowing parameter, b ~14 [20], that a small amount of N can cause a large reduction on Band gap energy [3, 4], the reduction results are mostly from the lowering of the conduction band., which represented by equation

$$E_{g(InGaPN)} = y.E_{g(InGaP)} + (1-y).E_{g(InGaN)} + b.y.(1-y) \qquad (2\text{-}13)$$

For a constant of In content (x) and y is the N content and b is the bowing parameter of InGaPN.

2.2 Solar Cell Application

For single absorber layer the theoretical efficiency limit to be about 40% for optimal bandgap absorber E_g = 1.1 eV. The major limitation is due to the thermalization loss which from the thermalization of hot carriers and non-adsorption loss which account approximately about 50% of incident solar energy [21]. For achieve higher efficiency, the multifunction solar cell is being introduced.

2.2.1 Multijunction Solar Cells

Multijunction solar cells are the solar cell that divide the absorber layer into multi-layer to collect the energy from solar spectrum. Each layer absorbs different energy range, the high bandgap or top cell convert the short wavelength fraction and permits the longer wavelength to convert at the lower cells or the lower bandgap in the stack layer. A schematic diagram of multijunction is illustrated in Fig 2-3. Because the cells are connected via p-n junction, this system is called multijunction solar cell. For this system, it is expected that the more number of p-n junctions, the less thermalization and transmission losses [22], resulting in high efficiency.

จุฬาลงกรณ์มหาวิทยาลัย
Chulalongkorn University

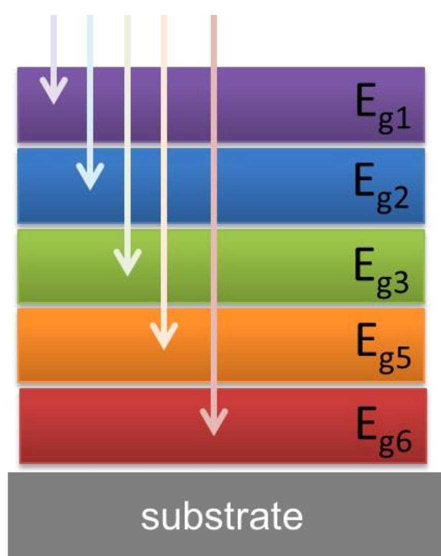

Fig. 2-3 Schematic drawing shows the light absorption of multijunction solar cell.

2.3 Ordering Effects

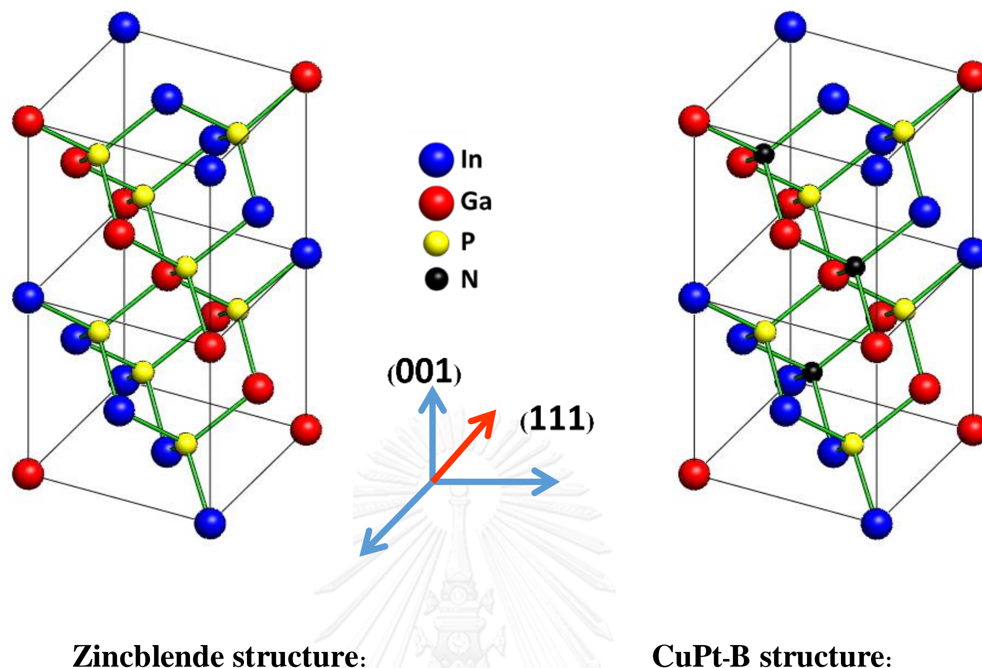

Fig. 2-4 InGaPN structure, Zincblende structure (Left) and CuPt-B structure (Right).

In the III-V alloys, such as InGaP and InGaPN, group-III and group-IV atoms distribute randomly on respective face center cubic (f.c.c) sub lattices (Fig2-4). When atoms of the alloys, e.g. Ga and In atoms in $In_xGa_{1-x}P$ distribute randomly on the group-III sub-lattice, material properties such as bandgap had been assumed to be a single-value function of alloy composition (x). it was noticed that the bandgap of In0.5Ga0.5P, which is a ternary alloy used as the active layer of the laser diode and is latticed-matched to the GaAs (001) substrate, had an anomalous lower value of 1.85 eV (at room temperature) than the most reliable value at 1.91-1.92 eV. The growth method used was metal organic vapor-phase epitaxy (MOVPE). And it was later found to depend on growth conditions such as ratio of group-III to Group-V pressure and growth

temperature. The searches for what kind of degree of freedom of the alloy system gives rise to this bandgap variation revealed an atomic ordering called CuPt-B ordering. The structure is a monolayer super-lattice of Ga-rich planes and In-rich planes ordered in the [$\bar{1}$ 1 1] or [1 $\bar{1}$ 1] directions (Fig 2-4). The degree of ordering corresponds qualitatively very well to the degree of bandgap anomaly. The correlation between ordering and the bandgap anomaly was later theoretically confirmed by the calculations of band structure. The theory clarified that the bandgap anomaly is due to the introduction of CuPt-B ordering, which introduces a periodicity double that of the Zincblende structure for the random alloy. The introduction of this crystal filed results in a Brillouin zone folding effect on the conduction-band structure and a crystal-field splitting effect on the valence band.

The calculation properties of the bandgap anomaly, due to the perfect ordering calculated by the theory, was significantly larger than the values obtained experimentally. The reason for this was further studied experimentally by using photoluminescence polarization spectroscopy, which has enabled quantitative estimations of the degree of ordering by measuring both of bandgap lowering and the valence-based splitting. Raman scattering spectroscopy has also detected this symmetry change in changes of the lattice vibration-spectrum. Among the several types of atomic ordering in III-V alloys, the CuPt-B type is the most important and most extensively studied. This is because it is the most dominant type of atomic ordering, and it occurs under very ordinary crystal-growth conditions.

The level of ordering in the material is denoted by its ordering parameter (η). A “completely disordered” or “completely random” alloy material has $\eta = 0$ while a

"completely ordered" material has $\eta = 1$. Thus, the ordering parameter is calculated from the following equation:

$$E_g(PL) = E_g^{(\eta=0)} - \Delta E_g^{(\eta=1)} \eta^2 \tag{2-14}$$

Where $E_g(PL)$ is the measured bandgap, $E_g^{(\eta=0)}$ and $\Delta E_g^{(\eta=1)}$ are the bandgap for "completely disordered" and splitting parameter for "completely ordered", respectively.

In case of InGaP(N), the degree of ordering can be describing by using Raman scattering. The valley-to-peak intensity ratio$\left(\frac{b}{a}\right)$, where a and b are shown in Fig. 2-5. A similar vibration mode of InGaP and InGaPN are observed. The spectrum has three peaks located. The sharp peak at 380 cm^{-1} (labeled as "C") is the GaP longitudinal optic (GaP-LO) phonon mode. The lower energy peak at 360 cm^{-1} (labeled as "B") is corresponding to the InP longitudinal optic (InP-LO) mode. Apart from the two LO modes, a broad structure at 330 cm^{-1} (labeled as "A") was allocated the InP transverse optic (InP-TO) mode, although it is forbidden in the ideal back scattering configuration in the zinc-blende structure. A weak signal due to the GaP-TO mode was reported [23] to exist at, 370 cm^{-1}, but this mode was probably screened by the InP-LO and GaP-LO modes in the spectrum of the most disordered samples. b/a ratio is related to inversely ordering parameter (η) which means

b/a = 1 › "completely disordering"

and

b/a = 0 › "completely ordering"

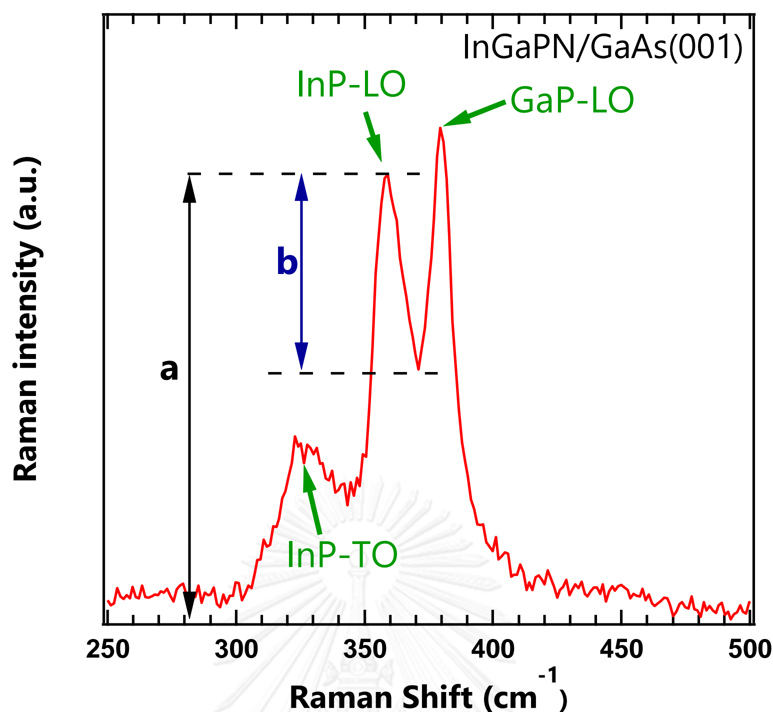

Fig. 2-5 The definitions of a and b from the InGaPN/GaAs Raman scattering.

In general, the b/a ratio was reported [13] to decrease from 0.5 in material with higher bandgap (more disordered) to 0.2 in material with lower bandgap (more ordered), and was attributed to the increasingly active GaP-TO mode at 371 cm $^{-1}$ because of cubic–trigonal transition in more ordered material. The valley depth reduction in increasingly ordered material is thought to be a result of increase in scattering by this mode.

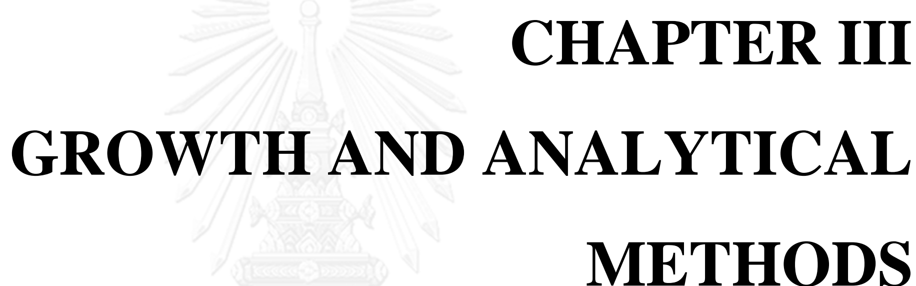

CHAPTER III
GROWTH AND ANALYTICAL METHODS

จุฬาลงกรณ์มหาวิทยาลัย

3.1 Metal Organic Chemical Vapor Phase Deposition (MOCVD)

Metal Organic Chemical Vapor Phase Deposition (MOCVD) is a highly complex process for growing a crystalline layer. MOCVD is a process that is used to deposit a very thin layers of atoms onto a semiconductor substrate. It is the most significant method for III-V compound semiconductors, especially for those based on Gallium Nitride (GaN).

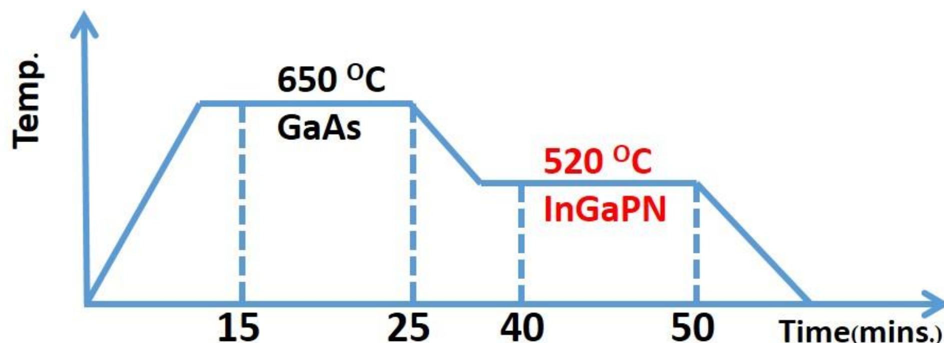

Fig. 3-1 Schematic of growth process of InGaPN.

3.1.1 Growth of Samples

All of the samples of this studied were grown at Onabe's laboratory, University of Tokyo, Japan. The $In_xGa_{1-x}P_{1-y}N_y$ films were grown on GaAs (001) substrates by vapor phase epitaxy (MOVPE) with trimethylgallium (TMGa), trimethylindium (TMIn), tertiarybutylphosphine (TBP), tertiarybutylasine (TBAs) and dimethylhydrazine (DMHy) as the precursor at 60 Torr and 2000 sccm, respectively. Before the InGaPN growth, the GaAs substrate was thermally cleaned at 650°C in TBAs atmosphere for 15 min. A 100-nm-thick GaAs layer grown at 650°C is used as a buffer. Growth temperature and growth time of InGaPN were 520°C and 10 min, respectively. To obtain the [TMIn]/([TMIn]+[TMGa]) mole fraction of 0.63, flow rates of TMIn and TMGa were respectively kept at 14.7 and 8.6 μmol/min for all the samples. Since, the [TMIn]/([TMIn]+[TMGa]) mole fraction of 0.63 is expected to make the compressive strain in the grown layer. To compensate the compressive strain, the N content was increased by varying DMHy flow rates in the range of 0 - 1,100 μmol/min. To improve the sample quality, the post-growth rapid thermal annealing (RTA) treatments were used and several different annealing conditions were tried. The sample with different DMHy flow rates (a) 300, (b) 700 and (c) 1,100 μmol/min were cut in to the four small parts. The annealing temperatures are held at 650 with halogen lamp in

N_2 ambient and the annealing duration was varied from 30 s to 180 s. Moreover, during annealing the GaAs wafer covered the samples to prevent any desorption of the group-V elements. All annealing processes were carried out in a nitrogen atmosphere.

3.2 Characterized Methods

In this work, several characterized methods were applied to InGaPN alloy films. Atomic Force Microscopy (AFM) and Secondary Electron Microscopy (SEM) were applied to investigate the surface and topography of the films. High Resolution X-ray Diffraction (HRXRD) and Raman scattering were characterized for investigated the structural properties and Photoluminescence for optical properties of InGaPN alloy films.

3.2.1 High Resolution X-ray Diffraction

High resolution X-ray diffraction (HRXRD) is the useful technique that uses the X-ray beam to investigation the lattice parameter and structural properties. The X-ray beam is focus and aimed to project on the sample and then is diffracted by the atomic in different planes in the sample. The d-spacing between the atomic planes cause the path difference of the diffracted X-ray beam and results in the diffraction patterns. The composition, the uniformity of each layer, their thickness, the built-in strain and strain relaxation, the lattice parameters and the lattice mismatch can be obtained by the diffraction pattern. There are possible five structure information's that can be obtained by HRXRD which are related to strain that occur for epitaxial film; a) lattice-matched, b) fully compressive strain, c) fully tensile strain d) partially relaxed and e) fully relaxed. The HRXRD results can determine those strain properties.

Chulalongkorn University

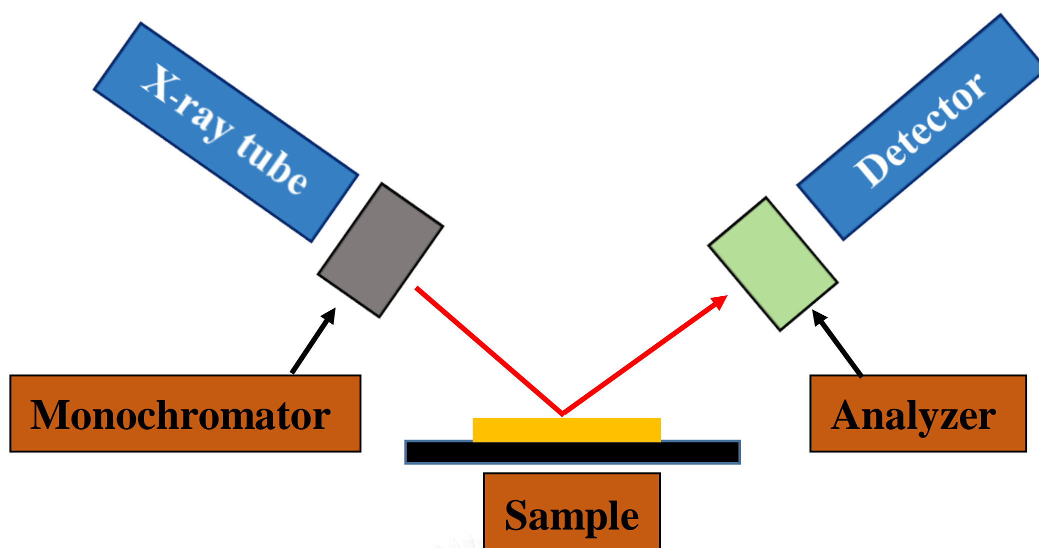

Fig. 3-2 Schematic of the High Resolution X-ray diffraction (HRXRD).

There are three important modes done for characterize the structural properties by HRXRD.

a) 2θ/ω-scan

In this mode, the Bragg angle is varied. The d-spacing of each layer can be distinguished. The different d-spacing is due to the different lattice parameters. Practically, the X-ray tube is fixed. The 2θ and ω angle are varied by moving the detector and sample, respectively. The information from this mode are related to the angle, ω, and the intensity of diffracted X-ray. The broadening of the layer peak is referred to the distribution of the orientation of the structure.

b) 2θ/ω-ω map and reciprocal space map

In this mode, the Bragg angle is varied (2θ/ω-scan). Moreover, the ω-scan is also done for each Bragg angle. Typically, the x-axis is 2θ range while the y-axis is ω range. The z-axis is the related intensity. Hence, this 3-axes graph contains the information about the lattice parameters, mosaic structure and strain of every layer in

the sample. This 2θ/ω-ω map can be converted to the reciprocal space (hkl) map and vice versa. The h and k are directly related to the in-plane lattice constant (a//) while l is related to the out of plane lattice constant ($a^{\perp}$). It is easy to observe the strain property from the reciprocal space map.

c) ω-scan or Rocking curve

In this mode, the value of 2θ is fixed while the ω is varied. The orientation of the intentional Bragg planes (ex. (004) plane) is observed. In the other word, the tilted mosaic structure is probed. Practically, the Bragg angle is fixed (the positions of the x-ray tube and detector are fixed) while the sample is rocked. The range of ω-scan is about 2 degrees. A graph of the intensity versus the ω angle is plotted. This graph is often called "rocking curve". This mode is usually to determine the lattice constant and the distribution of it lattice sized by the FWHM of the layer peak.

The combination HRXRD results from both symmetric plane, (004), and asymmetric plane, (115), provide the complete information of lattice parameters of the sample and hence the related composition. In this work, the experiments were done on Bruker HRXRD machine model Bruker AXS D8 Discovery at research institute, Chulalongkorn university which use copper (Cu) as the X-ray source and Germanium (Ge) (220) as monochromator to produce a 1.5406 Å $K_{\alpha 1}$.

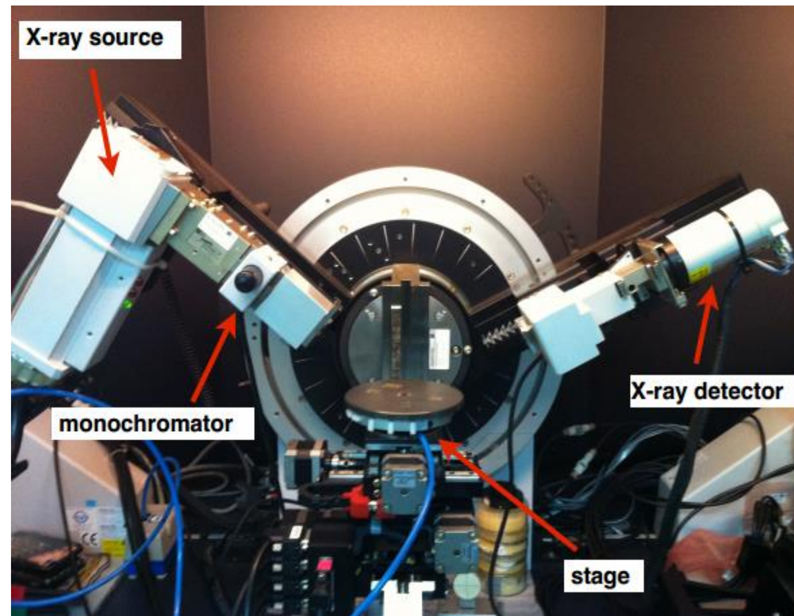

Fig. 3-3 Bruker AXS D8 Discovery HRXRD machine at at research institute, Chulalongkorn university.

3.2.2 Raman Scattering

When light is incident to the sample, some fraction is scattered. There are two possible processes for light scattering. First process is elastic scattering or Rayleigh scattering. In this process, the scattered photons have the same energy as the incident photons. Second process is the inelastic scattering or Raman scattering which the scattered photons have the energy different from the incident photons due to phonon creation or annihilation. The Raman scattering is divided into two cases, anti-Stokes and Stokes scattering which the scattered photons have the energy larger and smaller than the incident photons, respectively. Typically, Stokes scattering is chosen to measure because of higher intensity. The graph obtained from measurement is plotted between the Raman shift (cm^{-1}) and the intensity of scattered photons. The Raman shift is defined by

$$\text{Raman shift } (cm^{-1}) = \frac{1}{\lambda_{incident}} - \frac{1}{\lambda_{scattered}} \quad (3\text{-}1)$$

where $\lambda_{incident}$ and $\lambda_{scattered}$ are the wavelength of the incident and scattered photons, respectively. This value is related to the phonon energies of bonds in the sample.

In this research, the Raman measurement with back scattering geometry was performed. The geometry is simple shown in Fig. 3.10. For ideal back scattering geometry, the Raman selection rule not allows the transverse phonon vibration mode.

For III-V-N alloy, especially InGaP, Raman sift also verified the ordering effect by measuring valley-to-peak (b/a) intensity ratio

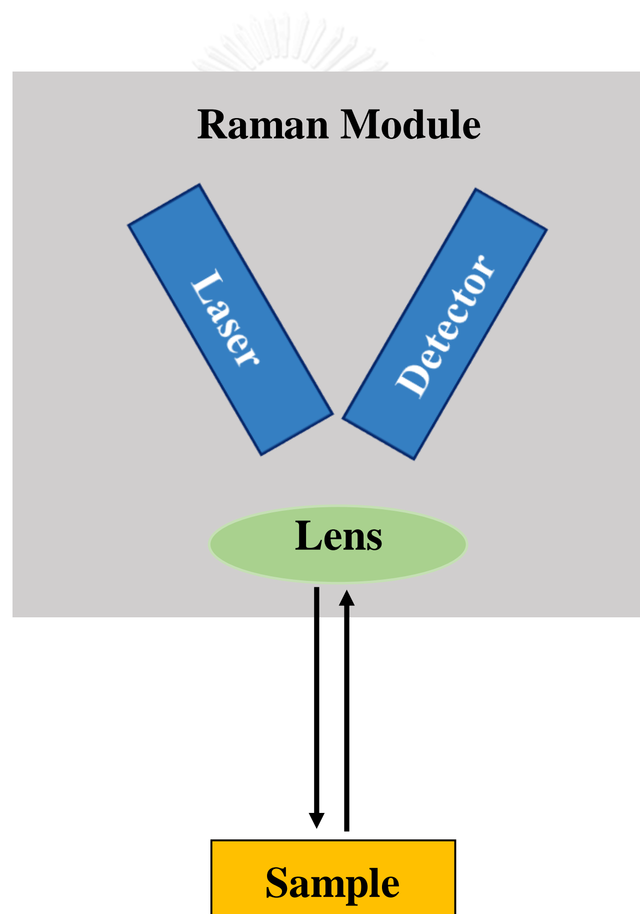

Fig. 3-4 Schematic of Raman scattering measurement with back scattering geometry.

3.2.3 Photoluminescence

Photoluminescence (PL) is the spontaneous emission of light from a material under optical excitation, that is, when monochromatic light or photon of which the energy is not smaller than the energy gap of the specimen is projected onto such specimen, electron-hole pairs are produced. The excited state, however, is unstable for electron. Accordingly, it is noted that the recombination of electron and hole are created and result in emission of excess energy, which is called “photoluminescence”. Feature of this energy spectrum can be used to examine the information about energy levels of the material such as bandgap level, impurity levels and defect related levels.

The room temperature Raman and the photoluminescence measurement were performed at The Gem and Jewelry Institute of Thailand (Public Organization). The argon ion laser with wavelength 514.5 nm was used to the excitation source. The spot size of the laser beam is about 2 μm. the CCD detector is used.

จุฬาลงกรณ์มหาวิทยาลัย
CHULALONGKORN UNIVERSITY

CHAPTER IV
RESULTS AND DISCUSSIONS

4.1 Alloy Composition Investigations of Nearly Lattice-Matched InGaPN Films

จุฬาลงกรณ์มหาวิทยาลัย
CHULALONGKORN UNIVERSITY

Due to the incorporation of N in InGaPN, The P atom, bigger atom sized, was replaced by the N atom, smaller atom sized, in the InGaP system. The different in the atom sized between these two atoms were cause a compressive-strained which results in suppression of the generation of misfit dislocation in the InGaPN alloy. And also the quaternary alloy composition of InGaPN has a complex to evaluate the alloy composition each, too.

In this topic, composition and strained of the InGaPN alloy on GaAs (001) substrate with N incorporation were evaluated. High-resolution X-ray diffraction

(HRXRD) $2\theta/\omega$ and mapping measurement were carried out to evaluate the strained of the InGaPN film and with a combination of Raman spectroscopy measurement the In and N concentrations in the epitaxial InGaPN alloy films will be determined.

The growth of InGaP(N) films on GaAs (001) substrates were established by HRXRD analysis using a symmetrical (004) 2θ/ω scan and an asymmetrical (115) reciprocal lattice mapping (RSM). Fig 4-1 shows HRXRD (004) 2θ/ω profiles for the InGaP(N) alloy films with different DMHy flow rates of (a) 0, (b) 300, (c) 700 and (d) 1,100 μmol/min. All the diffraction pattern consists of a well-defined diffraction peak located at 66.06°, which is referred to the GaAs (004) substrates reflection and a broaden curve at lower diffraction angles, indicating the InGaP(N) (004) reflections. This shows a reduction of the normal lattice parameter ($a_{\perp}$) due to the N incorporation. Besides, an increase of full width at half maximum (FWHM) with increasing DMHy flow rate is also clearly seen, demonstrating a less coherency of lattice spacing due to a large distribution of both the In and N contents in the InGaPN layers.

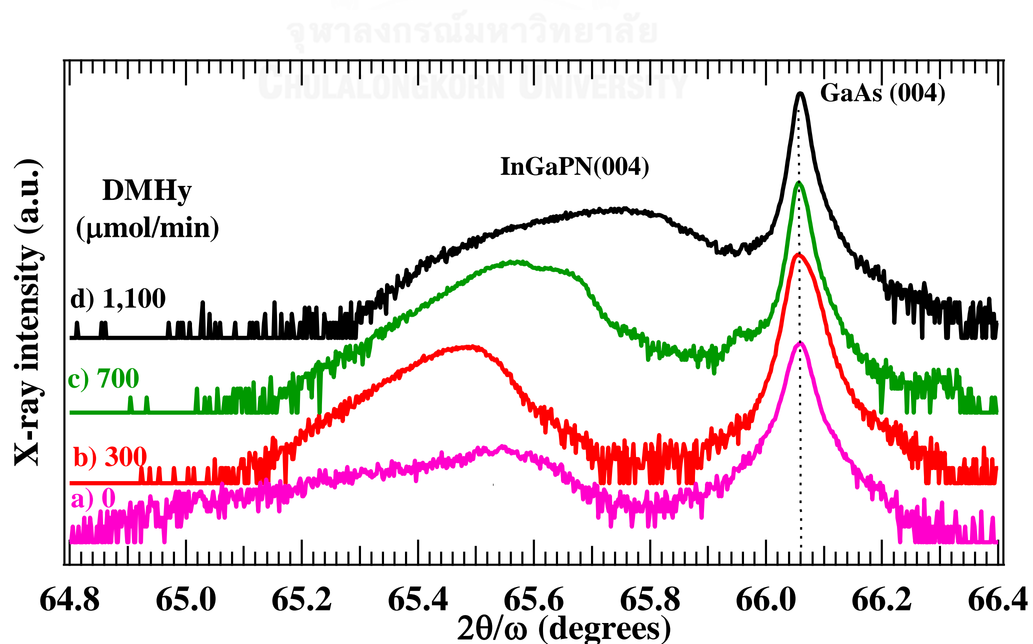

Fig. 4-1 HRXRD $2\theta/\omega$ profiles of (a) InGaP film and (b) – (d) InGaPN films grown on GaAs (001) substrates as dependent on DMHy flow rates.

Fig. 4-2 shows HRXRD reciprocal space maps taken around an asymmetric (115) reflection of (a) the N-free InGaP film and the InGaPN films with a DMHy flow rates of (b) 30, (c) 700 and (d) 1,100 μmol/min, respectively. It is seen that diffraction from both GaAs (115) and InGaPN (115) planes are clearly observed. The separation between the GaAs and InGaPN diffraction contours in ω-axis, "Δω", is corresponded to a tile angle between the GaAs (115) and InGaPN (115) planes. It is noted that Δω will be became zero for a fully relaxed film, which results in parallel GaAs (115)//InGaPN (115) planes. When the DMHy increase, the diffraction contour of InGaPN (115) show the trend that moving align orientation along the full strained line (dash line as shown in Fig. 4-4 (a) to GaAs (115). Thus at 1,100 μmol/min DMHy flow rate, the diffraction contours of GaAs (115) and InGaPN (115) planes are aligned along the fully strained line (dashed line), when the film exhibits as a coherently grown film, resulting in lattice-matching between lattice constant of GaAs and in-plane lattice parameter ($a_{\|}$). Thus, the grown film is under a fully strain condition. On the other hand, the separation in 2θ/ω-axis is resulted from the difference in lattice spacing, which is reduced with increasing DMHy flow rate. Furthermore, a rotation of the elliptic contour of the InGaPN (115) indicates an existence of a residual strain in the film. It is evidenced that, for the highest DMHy flow rate of 1,100 μmol/min, the InGaPN film is still under a compressive strain condition.

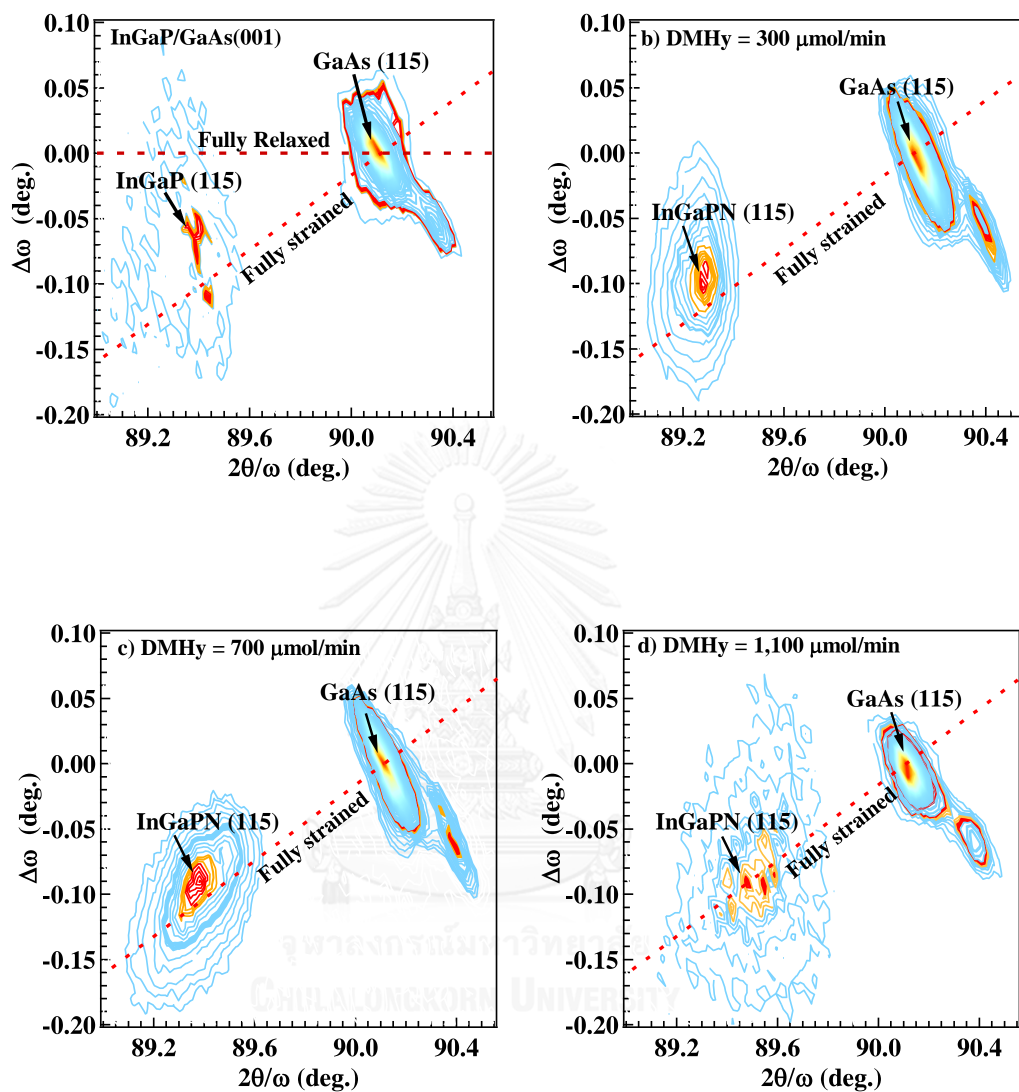

Fig. 4-2 HRXRD 2θ/ω and Δω reciprocal space maps around an asymmetrical (115) reflection for the InGaPN films on GaAs (001) substrates as dependent on the DMHy flow rates, (a) 0, (b) 300, (c) 700 and (d) 1,100 μmol/min.

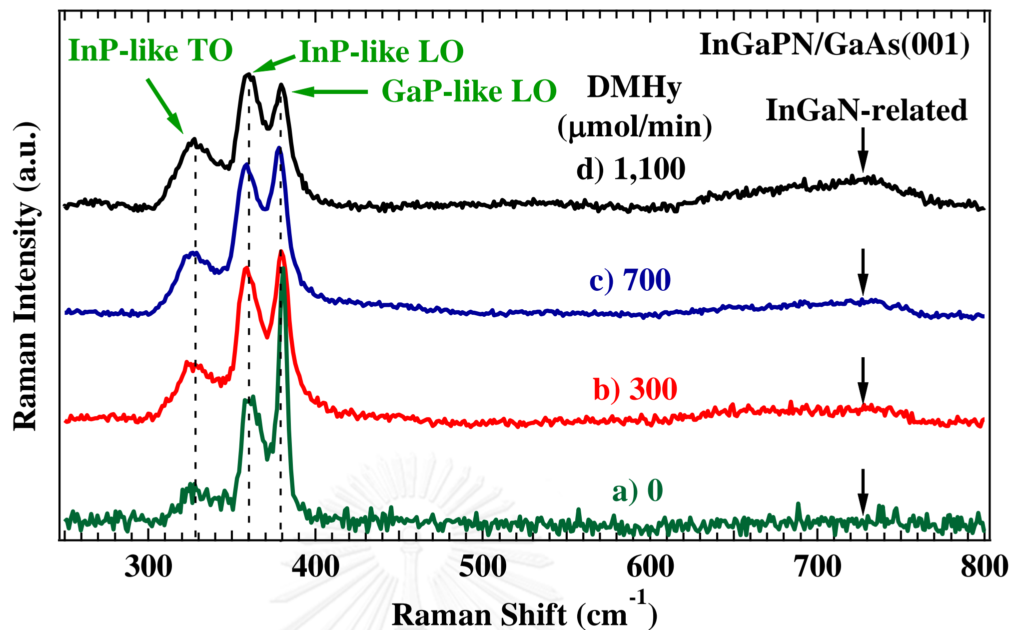

Fig. 4-3 Raman spectra of InGaPN films grown on GaAs (001) substrates with various DMHy flow rates of (a) 0, (b) 300, (c) 700 and (d) 1,100 μmol/min.

Fig. 4-3 illustrate Raman spectra of InGaPN films grown on GaAs (001) substrates with various DMHy flow rates of (b) 300, (c) 700 and (d) 1,100 μmol/min. The GaP-like LO, InP-like LO and InP-like TO phonons are also observed for all the InGaPN films. InGaPN also shows a partial two-mode behavior, LO and TO modes. The Raman selection rules not allows the transverse vibration mode for an ideal backscattering geometry. The observable of this mode might come from the small deviation of weak scattering geometry and fluctuation in the alloy [24]. In addition, another board feature related to N incorporation was observed at wave number around 730 cm^{-1}. With increasing DMHy flow rate, its intensity is significantly increased, indicating a higher amount of N incorporation into the InGaPN film.This feature is known as the InGaN-related local vibrational mode [25]. The vibration mode of Cubic GaN-LO and -TO be located at 742 and 555 cm^{-1}, while cubic InN-LO and -TO be

located at 586 and 472 cm^{-1}. The dominant peak around 730 cm^{-1} is close to the vibration mode of GaN-LO. Moreover, there is no peak that are observable about the InN vibration mode, 472 and 586 cm^{-1}. This suggests the N incorporation in InGaPN samples are contribute to form Ga-N bonds more than In-N bonds [26].

To analyze the In content, relaxed lattice constant (a_o), lattice mismatch and misfit strain in the N-free InGaP film, values of $a_\perp$ and $a_\parallel$ were firstly determined by a symmetric (004) 2θ/ω-scan and an asymmetric (115) RSM as shown in Fig 4-1 and 4-1 (a), respectively. According to Vergard's law, equation 2-6 and 2-8 in chapter 2, the In content and a_o were determined using the initial input parameters listed in Table 2-1. Thus, the In content and value of a_o were calculated to 56.6±1.7 at% and 5.65±0.01 Å, respectively. A large variation of In content (±1.7 at%) is due to a distribution of In concentration, which is larger than an instrumental error. The misfit strain, equation 2-1 in chapter 2, in InGaP layer was evaluated to be 0.65%.

Unfortunately, for the N-contained InGaPN films, the N content cannot be evaluated with using only the results obtained from HRXRD. It is due to a combination of four elements in such quaternary InGaPN alloy. Then, to calculate the N content, the In content is needed to be initially confirmed by another method that we selected micro-Raman scattering technique. It is well known that the In content in InGaP is significantly related to the optical phonon frequencies, especially GaP-like LO phonon reported by Bedel et al. [27]. A shift of GaP-like LO phonon frequency ($\Delta\omega_{GaP-like\ LO}$) as a function of the In content (x) is expressed as

$$\Delta\omega_{GaP-like\ LO} = -18.18x^2 - 38.97x. \qquad (4\text{-}1)$$

Here $\Delta\omega_{GaP-like\ LO}$ is a different between the frequencies of GaP- like LO phonon taken from InGaP compared to that of GaP-LO phonon taken from GaP (404.99

cm^{-1}). From the relation (4-1) we can evaluate the In content from InGaPN by using the Raman scattering spectroscopy.

Figure 4-3 (a) shows Raman spectrum of the N-free InGaP film on GaAs (001) substrate. The spectrum consists of three features located at the wave number of about 380, 360 and 330 cm^{-1}, which are attributed to GaP-like LO, InP-like LO and InP-like TO phonons, respectively. Therefore, we used the value of $\omega_{GaP-like\ LO}$ taken from the N-free InGaP film, as shown in Fig. 4-3 (a) to calculate the In content to be 56.4±0.8 at%. This result agrees well with that of HRXRD. Unlike the variation of In content (±1.7 at%) obtained from HRXRD, the value of ±0.8 at% obtained from micro-Raman scattering represents an error, which is introduced by a step size in wave-number axis.

According to GaP-like LO phonon frequencies, $\omega_{GaP-like\ LO}$, the In content in the InGaPN films was determined to 55.8±0.8 at%, 55.9±0.9 at% and 55.7±1.1 at% for the DMHy flow rates of 300, 700 and 1,100 µmol/min, respectively. It is seen that the In content in InGaPN is slightly lower than that in the N-free InGaP. This difference is due to a modification of a misfit strain in the N-contained InGaPN films. With a use of the In content calculated using the shift of GaP-like LO phonon and the normal ($a_{\perp}$) and in-plane ($a_{\parallel}$) lattice parameters obtained from HRXRD measurements, the N content in the InGaPN films can be acquired by the modified Vergard's law

$$a_{InGaPN} = \frac{2.C_{12}.a_{//}+C_{12}.a_{\perp}}{2.C_{12}+C_{11}} \tag{4-2}$$

$$a_{InGaPN} = (1-x)[(1-y)a_{GaP} + ya_{GaN}] + x[(1-y)a_{InP} + ya_{InN}] \tag{4-3}$$

$$C_{11} = \frac{(1-x)[(1-y)a_{GaP}C_{11}^{GaP}+ya_{GaN}C_{11}^{GaN}}{a_{InGaPN}} + \frac{x[(1-y)a_{InP}C_{11}^{InP}+ya_{InN}C_{11}^{InN}]}{a_{InGaPN}} \tag{4-4}$$

$$C_{12} = \frac{(1-x)[(1-y)a_{GaP}C_{12}^{GaP}+ya_{GaN}C_{12}^{GaN}}{a_{InGaPN}} + \frac{x[(1-y)a_{InP}C_{12}^{InP}+ya_{InN}C_{12}^{InN}]}{a_{InGaPN}} \tag{4-5}$$

จุฬาลงกรณ์มหาวิทยาลัย
Chulalongkorn University

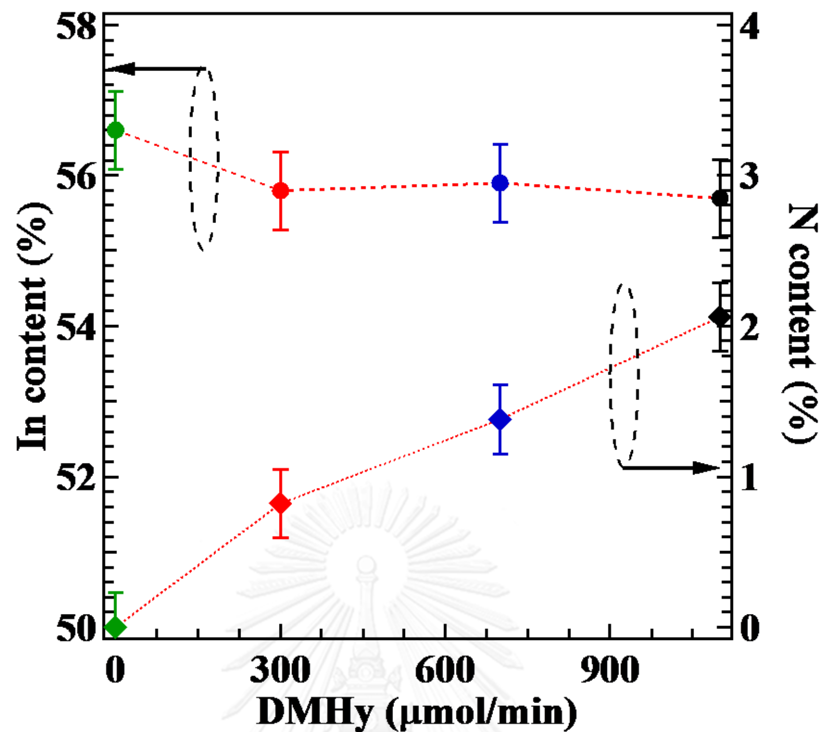

Fig. 4-4 The In and N content of the InGaPN films as dependent DMHy flow rates grown with [TMIn]/([TMIn]+[TMGa]) ratio of 0.63

Then, the N contents, which was successfully calculated using an interpolation method via Vergard's law, are 0.9±0.4 at%,1.4±0.4 at% and 2.1±0.5% for the InGaPN films with DMHy flow rates of 300, 700 and 1,100 µmol/min, respectively. The N content and the misfit strain of InGaPN films were evacuated, as show in Table 4-1. Fig. 4-4 shows a plots of the N and In contents as dependent on DMHy flow rates. With increasing DMHy flow rate from 0 to 1,100 µmol/min, the N content is increased from 0 to 2.1±0.5 at%. The distribution of the In is calculate from the distribution of the In for each located by 2 µm^2 of the Raman detector. The distribution of the N is 0.5% is calculated from the distribution of the In content from the Raman spectroscopy.

It is observed that, as the highest N content of 2.1±0.5 at%, the InGaPN grown layer is becoming a nearly lattice-matched film with the lowest misfit strain of 0.12%, which is about five times smaller than that of the N-free InGaP film. It is known that

Table 4-1 Relaxed lattice constant (a_o), misfit strain ($\varepsilon_{\|}$) and In content determined by micro-Raman spectroscopy) and calculated N content. Noted that the In content determined by HRXRD is 56.6±1.7 at%.

DMHy (µmol/min)	GaP-LO (cm^{-1})	$a_{\perp}$ (Å)	$a_{\|}$ (Å)	a_o (Å)	Misfit strain (%)	In (%)	N (%)
0	378.2±0.5	5.71	5.67	5.69	0.65	56.4±0.8	-
300	378.7±0.5	5.70	5.66	5.68	0.47	55.8±0.8	0.9±0.4
700	378.6±0.6	5.69	5.65	5.67	0.30	55.9±0.9	1.4±0.4
1,100	378.7±0.6	5.67	5.65	5.66	0.12	55.7±1.1	2.1±0.5

the lattice-matching condition between film and substrate prevents the epitaxial layer from a misfit dislocation, which degrade the quality of the grown layer. A nearly lattice-matched InGaPN on GaAs with a good quality were coherently grown by MOVPE with the In and N contents of 55.7±1.1 at% and 2.1±0.5 at%, respectively.

An adding N incorporation in InGaPN caused a reduction of an In incorporation and variation of the lattice constant. A combination of HRXRD and Raman spectroscopy measurements has been proposed to evaluate the In and N contents in the nearly lattice-matched InGaPN films grown on GaAs (001) substrates. According to Raman scattering results, the In content was calculated to be 56.4±0.8 at%, 55.8±0.8 at%, 55.9±0.9 at% and 55.7±1.1 at% for InGaPN films with DHMy flow rates of 0, 300, 700 and 1,100 µmol/min, respectively. An incorporation of N significantly influenced on a misfit strain in the InGaPN films, which is significantly reduced with increasing N content. We achieved a nearly lattice-matched InGaPN film to GaAs with the lowest magnitude of misfit strain of 0.12%.

4.2 Effect of N Incorporation on Alloy Fluctuation, Ordering Effect and Non-radiative Recombination Center in InGaPN on GaAs Substrate

4.2.1 Surface Morphology and Alloy Fluctuation

Fig. 4-5 show the surface morphology of the InGaP(N) alloy films which observed by atomic force microscopy (AFM) with a scanning area of 10x10 μm^2. The InGaP(N) alloy films were grown on GaAs (001) substrate with the various DMHy flow rates of (a) 0, (b) 300, (c) 700 and (d) 1,100 μmol/min. It is clear that the surface of all the InGaPN films shows the island-like features with an elliptic shape, which is aligned in an elongate the [110] direction. The elongate sized of the ellipse show a decreasing as increased the DMHy flow rates. The surface roughness Root Means Square (RMS) was measured 8.9, 10.7, 10.8 and 25.2 nm for DMHy flow rates 0, 300, 700 and 1,100 μmol/min, respectively. The value of surface roughness RMS is quite similar the same for 300 and 700 μmol/min DMHy flow rates. However, at 1,100 μmol/min, the roughness RMS is dramatically increased up to 25.2 nm. A formation of the elliptic shaped structure and surface roughness RMS may be resulting from decreasing of a migration length due to a large value of [TMIn]/([TMIn]+[TMGa]) as well as a presence of DMHy during the growth. The higher concentration of DMHy cause a change the formation form 2D to 3D islands.

Fig. 4-6 show the surface of the InGaP(N) by the scanning electron microscopy (SEM). The shape of the surface domains show the shape as describe in the AFM surface morphology. The longer and wider shape of the surface due to the increasing DMHy flow rate can be explained by the decreasing of the diffusion length due to the high concentration of DMHy.

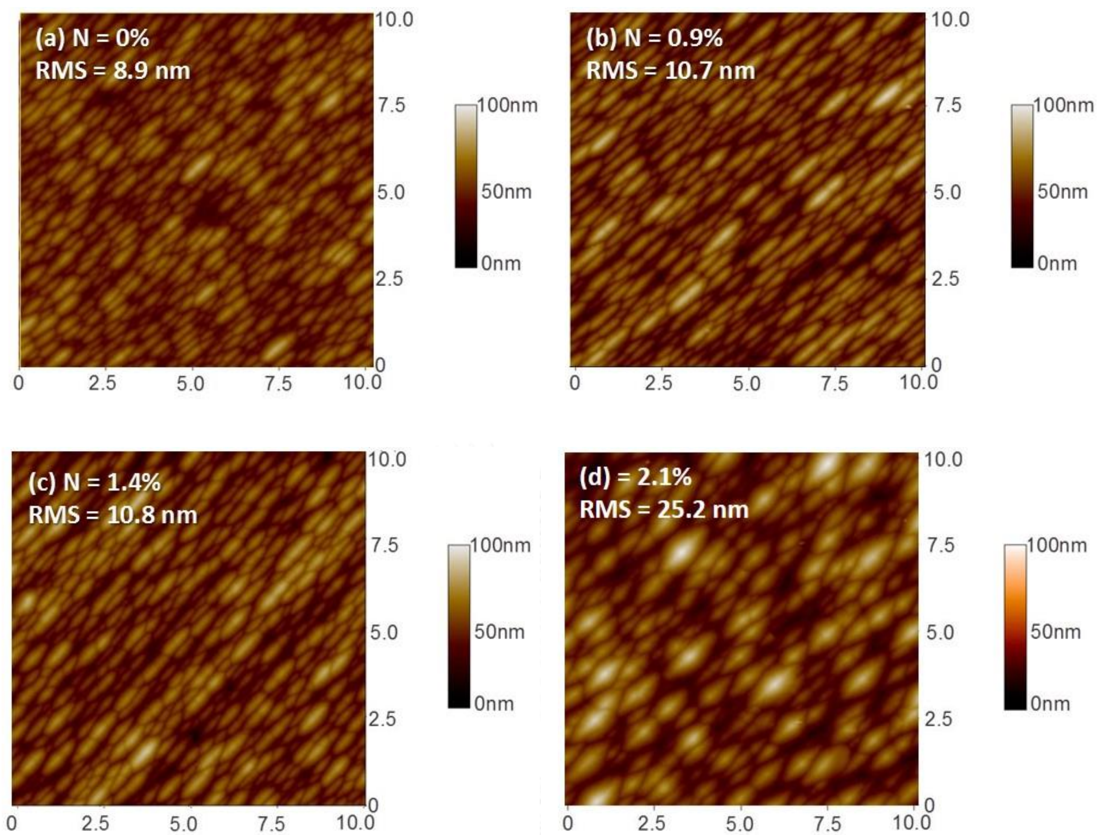

Fig. 4-5 show the surface morphology of the InGaP(N) alloy films which observed by atomic force microscopy (AFM) with a scanning area of 10x10 μm^2 of DMHy (a) 0 (b) 300, (c) 700 and (d) 1,100 μmol/min.

Chulalongkorn University

Fig. 4-7 show cross-sectional SEM images of the corresponding InGaPN film with thickness of about 0.7 μm taken with secondary electron imaging (SEI) and back-scattering imaging modes, respectively. Abrupt interface between InGaPN film and GaAs substrate are clearly observed even though the DMHy flow rate as high as 1,100 μmole/min. This indicates a high quality interface, which is avoided from a strain relaxation at the interface, due to a small amount of misfit strain.

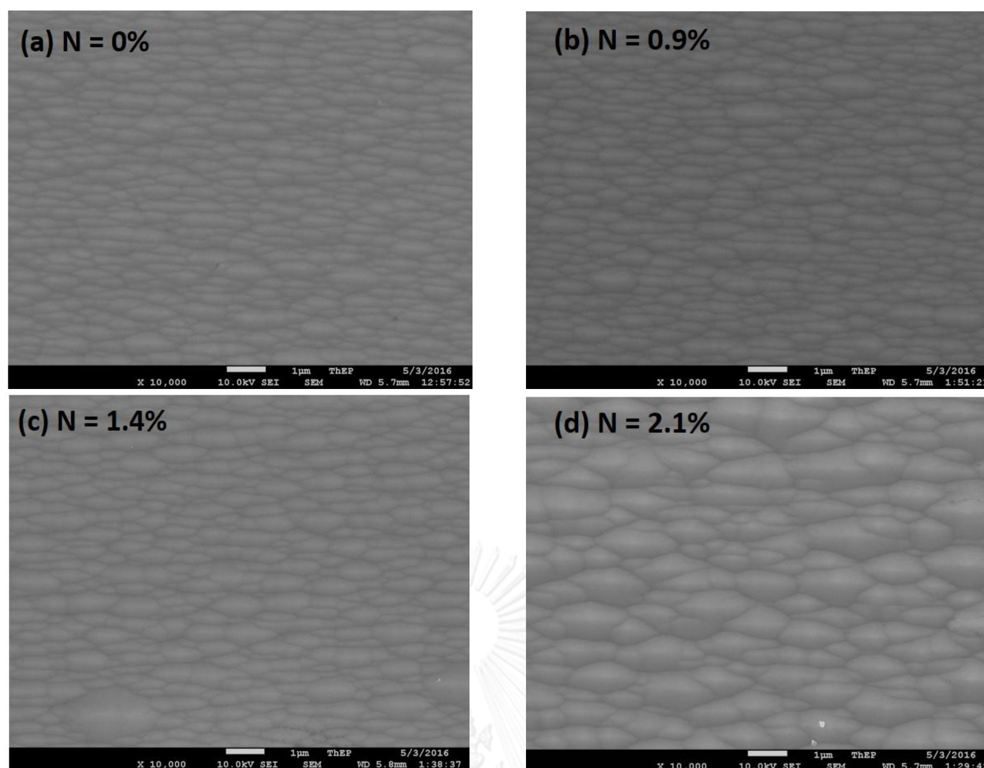

Fig. 4-6 show the surface morphology of the InGaP(N) alloy films which observed by scanning electron microscope (SEM) with a scanning of DMHy (a) 0 (b) 300, (c) 700 and (d) 1,100 µmol/min.

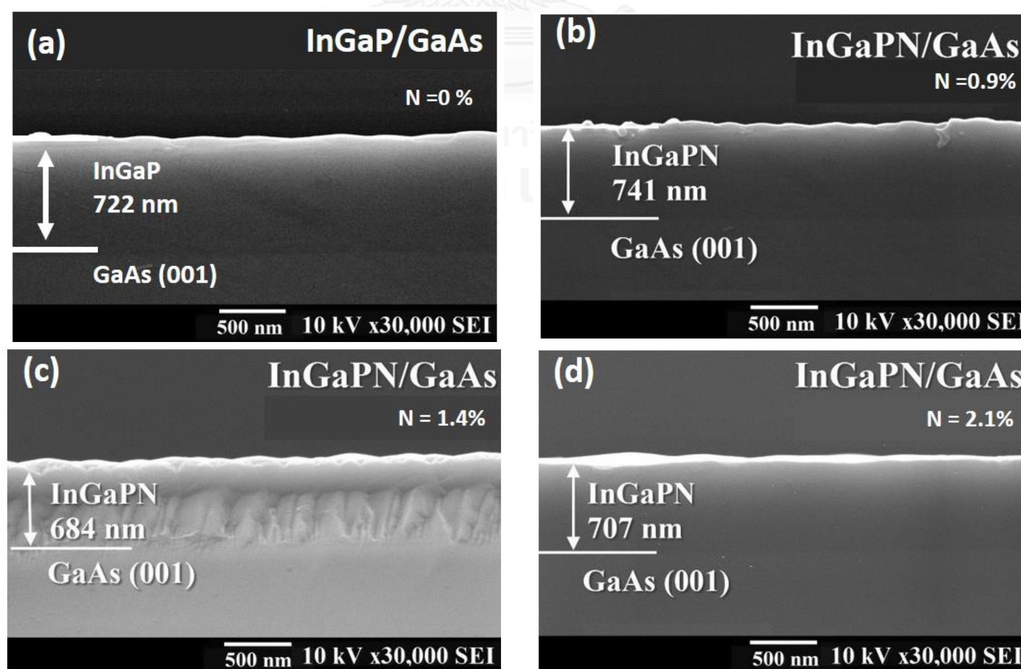

Fig. 4-7 show cross-sectional SEM images of the corresponding InGaPN film with thickness of DMHy (a) 0, (b) 300, (c) 700 and (d) 1,100 µmol/min.

4.2.2 Ordering Effect on N Contents

InGaPN showed a variation of band gap energy from the atomic different orientation in a crystal structures, ordering effected, that is influenced from growth parameters, such as III-V ratio, growth rate, substrate orientation and temperature. This effect causes a reduction in the band gap energy which splitting of the valence band and can affect the electronic and optical properties of the material [11, 25, 28].

Figure 4-8. show the $InGaP_{1-y}N_y$ layers Raman spectra in 250 – 500 cm^{-1} region with N contents of (a) N-free InGaP and InGaPN with various N contents (b) 0.9%, (c) 1.4% and (d) 2.1%. A similar vibration mode of InGaP and InGaPN are observed. The spectrum has three peaks located at ~380, ~360 and ~330 cm^{-1} as represent by GaP-LO, InP-LO and InP-TO phonon peaks, respectively. $InGaP_{1-y}N_y$ also shows a partial two-mode behavior, LO and TO modes. The Raman selection rules not allows the transverse vibration mode for an ideal backscattering geometry, the observable of this mode migh

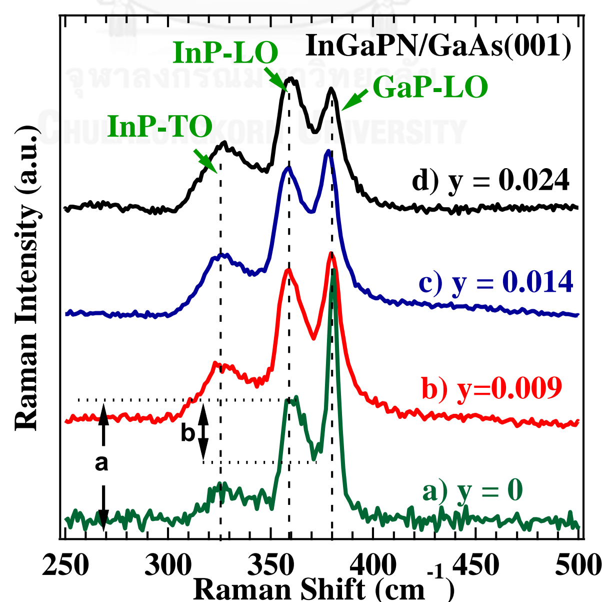

Fig. 4-8 Raman spectra of (a) N-free InGaP and InGaPN films grown on GaAs (001) substrates with various N contents (b) 0.9%, (c) 1.4% and (d) 2.1%.

come from the small deviation of weak scattering geometry and fluctuation in the alloy. The b/a ratios are a ratio of the depth of the valley between the GaP-TO phonon peak and the InP-LO phonon peak to the InP-LO phonon peak as shown in Fig 4-8. The invert relation between b/a ratio and ordering parameter (η) of InGaP in the region of weak ordering, η = 0.19 to 0.26, whereas the b/a is in the range of 0.43 to 0.32 were evaluated by Yoon et al [11].

Table 4-2 show the decreasing energy due to the ordering parameter can be calculated by

$$E_g(PL) = E_g^{(\eta=0)} - \Delta E_g^{(\eta=1)}\eta^2 \qquad (4\text{-}6)$$

where $E_g(PL)$ is the measured bandgap, $E_g^{(\eta=0)}$ and $\Delta E_g^{(\eta=1)}$ are the bandgap for "completely disordered" and splitting parameter for "completely ordered", respectively.

Table 4-2 b/a ratio, ordering parameter (η), band-gap energy (E_g) and $\Delta E_g^{(\eta=1)}\eta^2$ of InGaP(N)

Samples	N content (%)	b/a ratio	η	E_g (eV)	$\Delta E_g^{(\eta=1)}\eta^2$ (eV)
(a) InGaP	-	0.43	0.19	1.905	0.015
(b) InGaPN	0.9	0.41	0.20	1.848	0.017
(c) InGaPN	1.4	0.39	0.21	1.823	0.019
(d) InGaPN	2.1	0.32	0.26	1.798	0.029

Chulalongkorn University

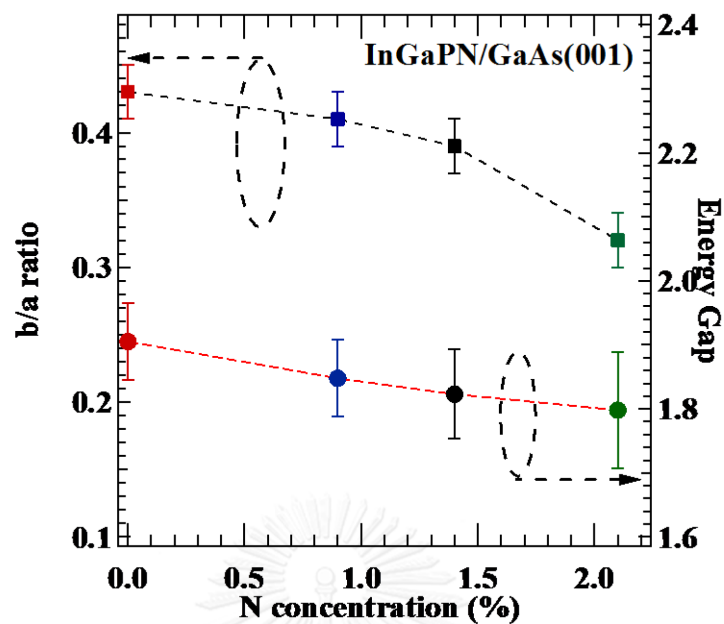

Fig. 4-9 b/a ratio and band-gap energy as the function of N contents of N-free InGaP and InGaPN with various N contents 0.9%, 1.4% and 2.1%.

As the results show in table 4-2, the highest of the ordering parameter (η) is 0.26 will cause the band-gap energy reduction about 29 meV. Comparing to the band-gap energy distribution due to the alloy fluctuation by micro-PL which is about ±30 meV which is larger than the band-gap reduced by the ordering effect. Thus, an ordering parameter is one parameter that show the significant effect on the reduction of the band-gap energy when the increasing N content.

4.2.3 Non-radiative Recombination Center

Fig. 4-10 show room-temperature photoluminescence spectra for (a) the N-free InGaP and the InGaPN film with DMHy flow rates (b) 300, (c) 700 and (d) 1,100 μmol/min, respectively. For $InGaP_{1-y}N_y$, the PL spectrum is dominated by abroad peak which a lower-energy shift of the PL peak position and a reduction in the PL peak intensity were also clearly observed with increasing N concentration (y). The reduction of the PL intensity indicating the presence of non-radiative recombination centers as a result of an increasing N incorporation. From the results, the intensity of the InGaPN with N content y = 2.1% is reduce about 12 time of the N-free InGaP, while a small amount N content y = 0.9% the PL intensity is almost the same with N-free InGaP. When N content increases from the N-free sample, y = 0% to y = 2.1%, the PL peak energy shifts to 1.85 eV, 1.82 and 1.80 eV for N contents of 0.9%, 1.4% and 2.1%, respectively, from 1.91 eV for the N-free sample. The red-shift amounts to ~ 57 meV, ~82 meV and ~ 107 meV for the films with N contents of 0.9%, 1.4% and 2.1%, respectively. Such a large red shift can be explained by the huge band gap bowing parameter, which is characteristic of III-V-N ternary alloys [29-32]. Fig. 4-11 show the band-gap energy plot as N content function which a bowing parameter for InGaPN 8-14 eV. The results are in the range of bowing parameter b = 8eV which indicated that the band-gap energy reduction is mainly from the alloy composition. The FWHM of the PL peak increase when more N add to InGaPN which suggested that an increase of alloy fluctuation.

จุฬาลงกรณ์มหาวิทยาลัย
Chulalongkorn University

Table 4-3 show the band-gap energy, FWHM and the integrate intensity ratio of an InGaPN on InGaP

Samples	N content (%)	E_g (eV)	FWHM	$\frac{I_{InGaP(N)}}{I_{InGaP}}$
(a) InGaP	-	**1.91 ± 0.02**	**0.04**	**1.00**
(b) InGaPN	**0.9 ± 0.4**	**1.85± 0.02**	**0.04**	**0.86**
(c) InGaPN	**1.4 ± 0.4**	**1.82± 0.02**	**0.05**	**0.65**
(d) InGaPN	**2.1 ± 0.5**	**1.80± 0.03**	**0.06**	**0.08**

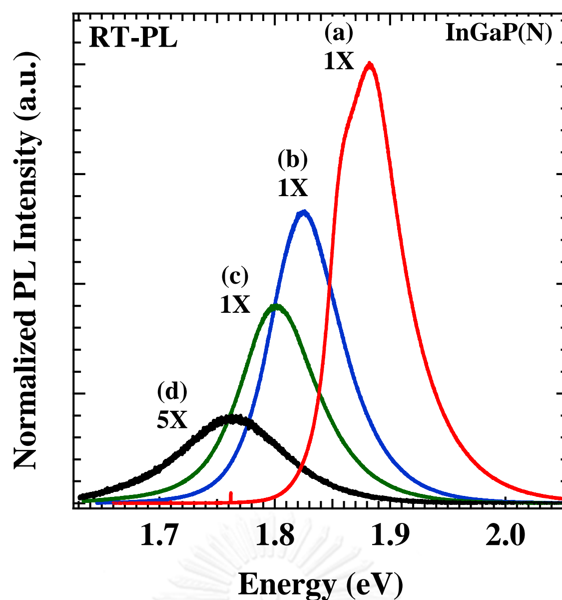

Fig. 4-10 a room-temperature PL of (a) N-free InGaP and InGaPN with various N contents (b) 0.9%, (c) 1.4% and (d) 2.1%.

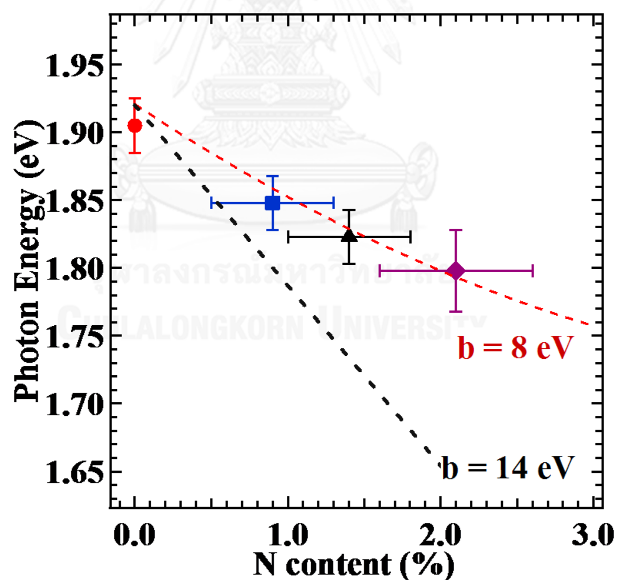

Fig. 4-11 band-gap energy of (●) N-free InGaP and InGaPN with various N contents (■) 0.9%, (▲) 1.4% and (♦) 2.1%.

4.3 Effects of Rapid Thermal Annealing on Alloy Fluctuation, Ordering Effect and Non-radiative Recombination Center of InGaPN on GaAs

The small amount of N incorporation in InGaPN can cause the electron captor defect and the decrease the luminescence intensity and broadening of the full wide at half maximum (FWHM) of photoluminescence (PL). However, we can improve significantly by using the post-growth treatment [33], such as post-growth rapid thermal annealing (RTA). RTA is usually performed on quaternary alloys to remove non-radiative defects and enhance their luminescence intensity with narrower FWHM of luminescence line.

4.3.1 Surface Morphology and Alloy Fluctuation after RTA

The surface morphology of InGaPN alloy films with varied DMHy flow rates 300, 700 and 1,100 µmol/min of as grown and annealed InGaPN with varied the annealing times 0, 30, 60, 120 and 180 seconds at annealing temperature 650 ^{O}C were observed by AFM as shown in Fig 4-13 for DMHy 300 µmol/min, Fig 4-14 for DMHy 700 µmol/min and Fig 4-15 for DMHy 1,100 µmol/min. The shape of the atom of the annealed samples at the surface are look like the same shape of as grown sample. The results of all surface RMS are plot as the function of annealing time as show in Fig. 4-12. The surface roughness RMS for DMHy 300 and 1,100 µmol/min show the same trend that the surface roughness RMS is slightly reduced when the annealing time is increased from as grown sample up to 120 s. Annealed samples after that the surface roughness dramatically increased when increase the annealing time up to 180 s. For 700 DMHy flow rate, the surface roughness RMS quit similar for all time of annealing. In the range of 0 -120 s. annealing time, the atom at the surface gain the thermal energy

from the annealing process to re-arrange the position of itself by the mass transportation at the surface that cause the surface roughness RMS are reduces. By the way when we annealing samples with the longer time, 180s, the long annealing time cause an increase of diffusion length with an high temperature of an annealing the formation of the tom change to 2D to 3D islands and some atom are diffused from the surface that cause the increase the surface roughness RMS.

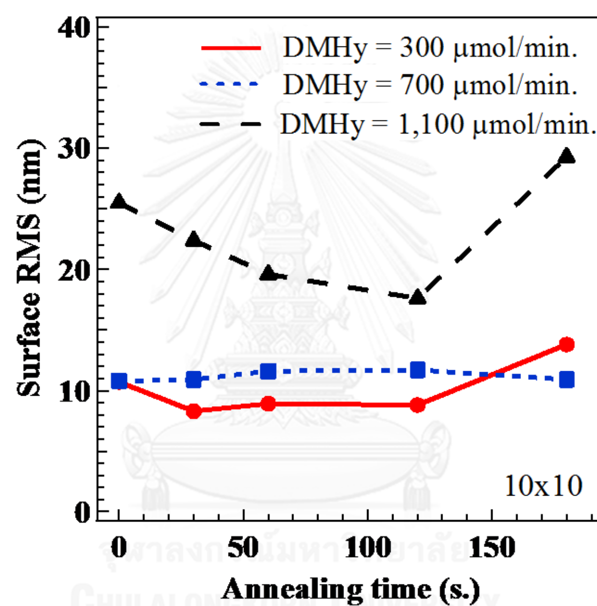

Fig. 4-12 show surface RMS as the annealing time function of InGaPN.

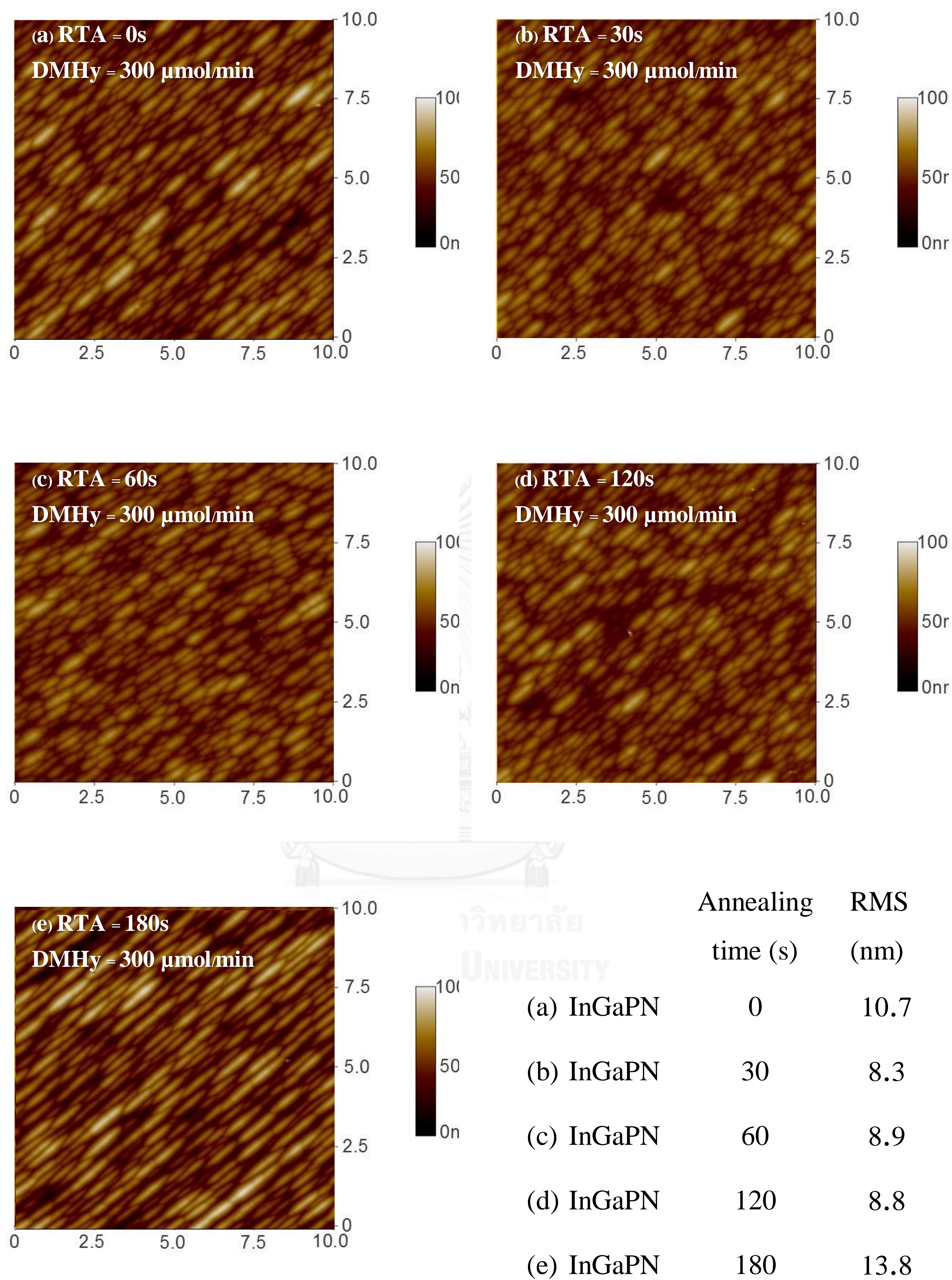

	Annealing time (s)	RMS (nm)
(a) InGaPN	0	10.7
(b) InGaPN	30	8.3
(c) InGaPN	60	8.9
(d) InGaPN	120	8.8
(e) InGaPN	180	13.8

Fig. 4-13 AFM images of the $In_xGa_{1-x}P_{1-y}N_y$ alloys films with DMHy 300 µmol/min grown on the GaAs (001) substrates rapid thermal annealing at annealing temperature 650 ^{O}C with varied the annealing times.

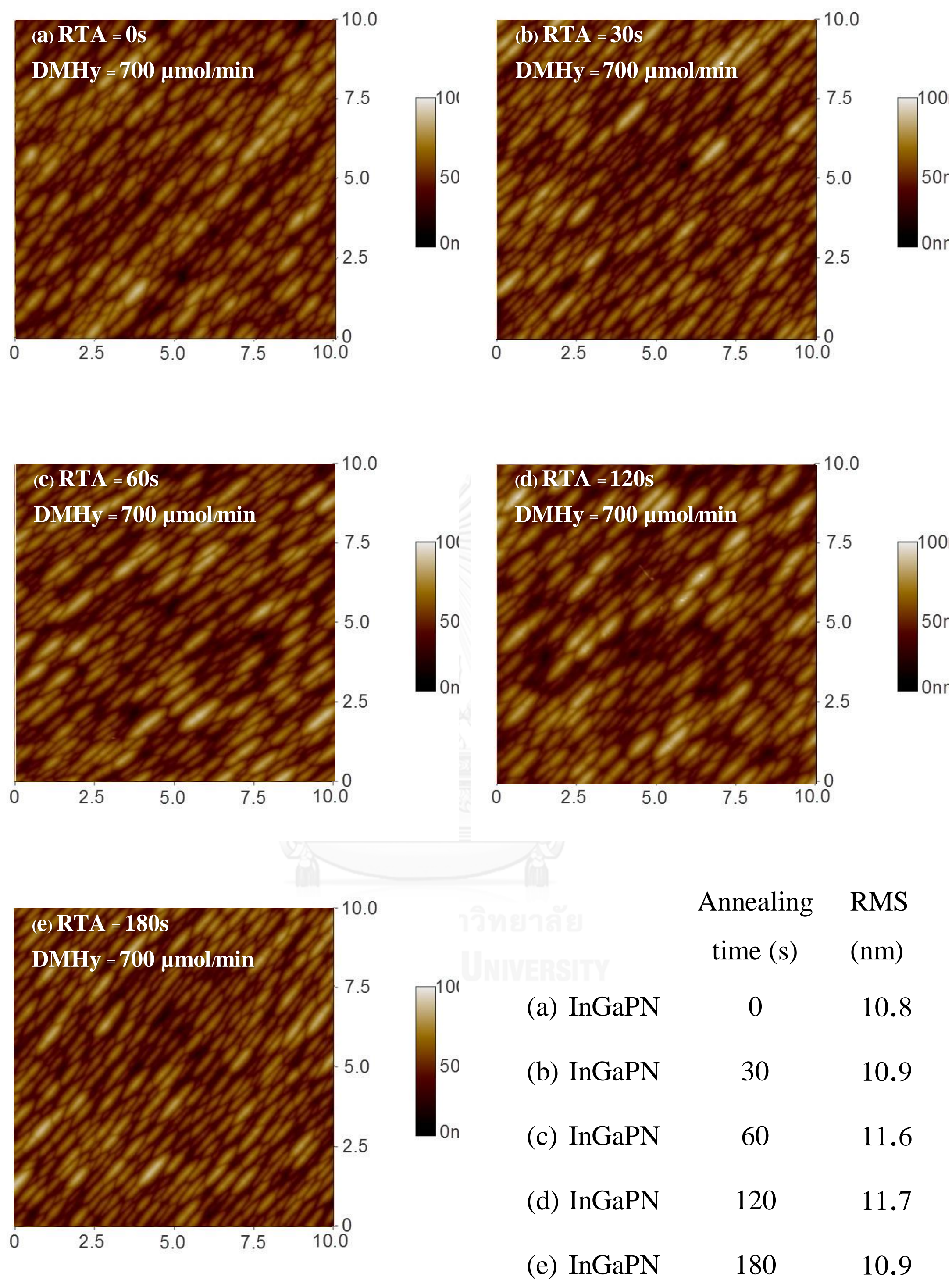

	Annealing time (s)	RMS (nm)
(a) InGaPN	0	10.8
(b) InGaPN	30	10.9
(c) InGaPN	60	11.6
(d) InGaPN	120	11.7
(e) InGaPN	180	10.9

Fig. 4-14 AFM images of the $In_xGa_{1-x}P_{1-y}N_y$ alloys films with DMHy 700 µmol/min grown on the GaAs (001) substrates rapid thermal annealing at annealing temperature 650 ^{O}C with varied the annealing times.

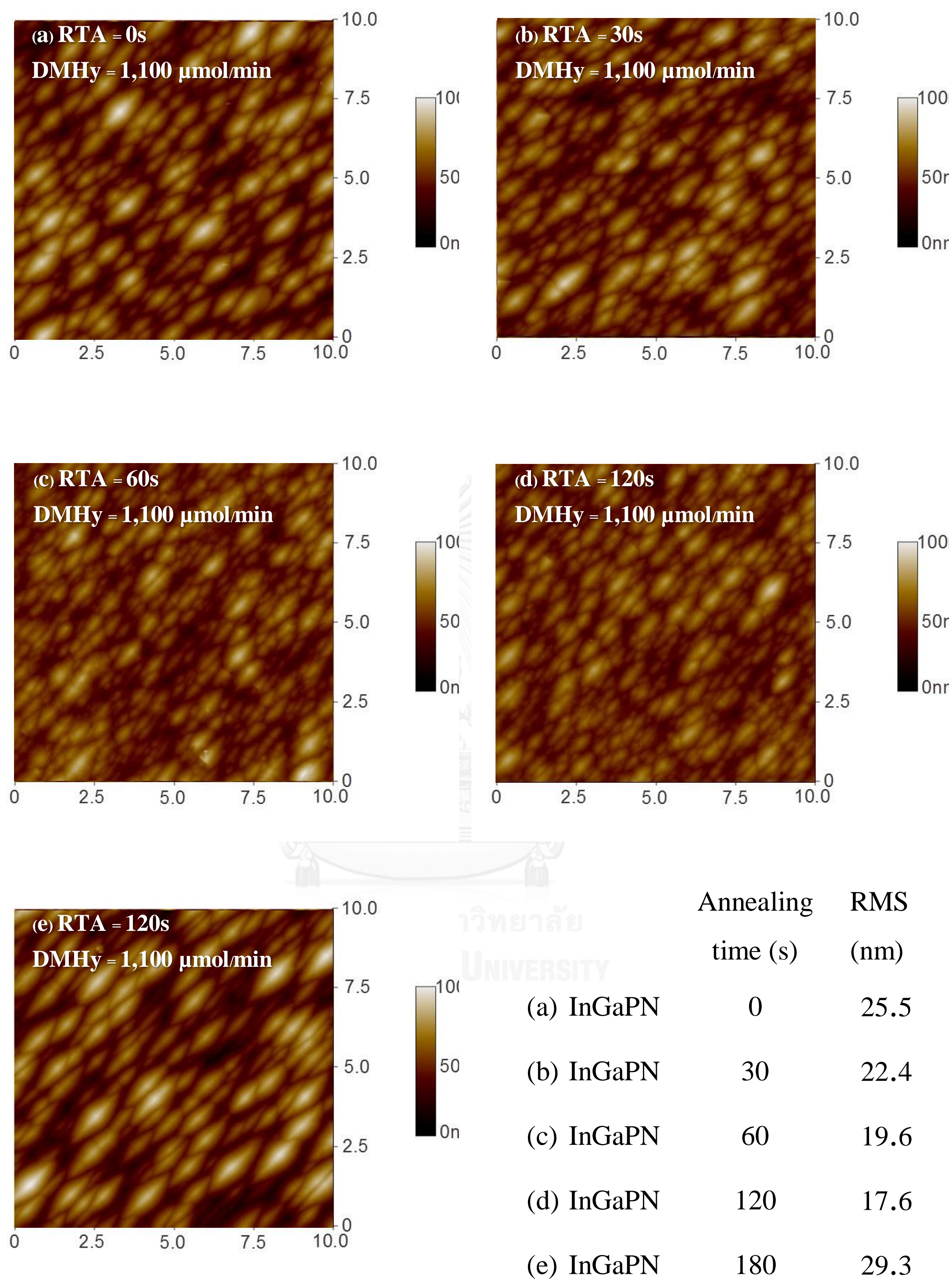

	Annealing time (s)	RMS (nm)
(a) InGaPN	0	25.5
(b) InGaPN	30	22.4
(c) InGaPN	60	19.6
(d) InGaPN	120	17.6
(e) InGaPN	180	29.3

Fig. 4-15 AFM images of the $In_xGa_{1-x}P_{1-y}N_y$ alloys films with DMHy 1,100 µmol/min grown on the GaAs (001) substrates rapid thermal annealing at annealing temperature 650 ^{O}C with varied the annealing times.

4.3.2 Alloy Composition after RTA

The post-growth rapid thermal annealing process was applied to InGaPN films on GaAs (001) substrates with various the DMHy flow rates 300, 700 and 1,100μmol/min. Fig 4-16 show HRXRD (004) 2θ/ω profiles for the InGaPN alloy films

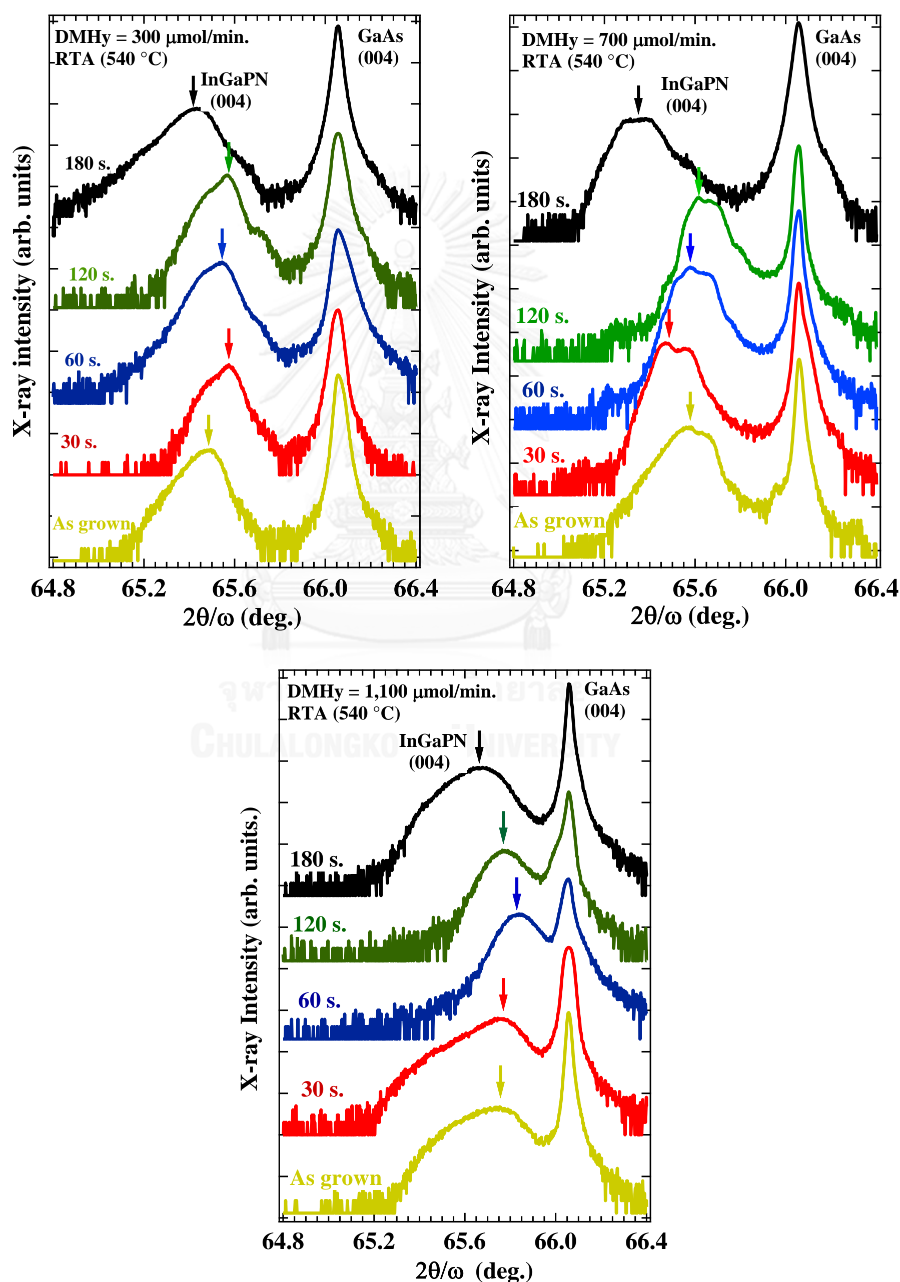

Fig. 4-16 HRXRD (004) $2\theta/\omega$ curves of $In_xGa_{1-x}P_{1-y}N_y$ alloys films grown on GaAs (001) substrates with varied the DMHy flow rate (a) 300, (b) 700 and (c) 1,100 μmol/min at different annealing time 0 – 180 s. at annealing temperature 650 ^{O}C.

with different DMHy flow rates of (a) 300, (b) 700 and (c) 1,100 μmol/min, respectively. The different annealing times were applied to as grown InGaPN samples at 30, 60, 120, and 180 s. as indicated in the graph for each DHMy flow rates. The diffraction pattern looks similar for as grown and annealed samples which consists of a well-defined diffraction peak located at 66.06^{o}, which is referred to the GaAs (004) substrates reflection and a broaden curve at lower diffraction angles, indicating the InGaPN (004) reflections. Compared to the as grown sample, the InGaPN (004) reflection peak shifts to the higher angles with increasing annealing time up to 120 s. However, at 180 s of annealing time, the InGaPN (004) reflection peak shifts back to the lower angle. The shift of the InGaPN (004) reflection peak come from their alloy composition changed, as describe in alloy composition change due to the increased DHMy flow rate, the shifted of the InGaPN (004) reflection are mainly from the N content in the InGaPN layers. Thus, the shifted of annealed InGaPN (004) reflection peak also mainly come from the N contents changed which an increase of N content leading to the higher angle shifted. By the way, a decreased of N content leading to lower angle shifted.

Fig. 4-17, 4-18 and 4-19 show HRXRD reciprocal space maps taken around an asymmetric (115) reflection of the InGaPN alloy films with different DMHy flow rates of (a) 300, (b) 700 and (c) 1,100 μmol/min, respectively. The different annealing times were applied to as grown InGaPN samples at 30, 60, 120, and 180 s. as indicated in the graph for each DHMy flow rates. It is seen that diffraction from InGaPN (115) planes are clearly observed similar to the as grown sample.

Chulalongkorn University

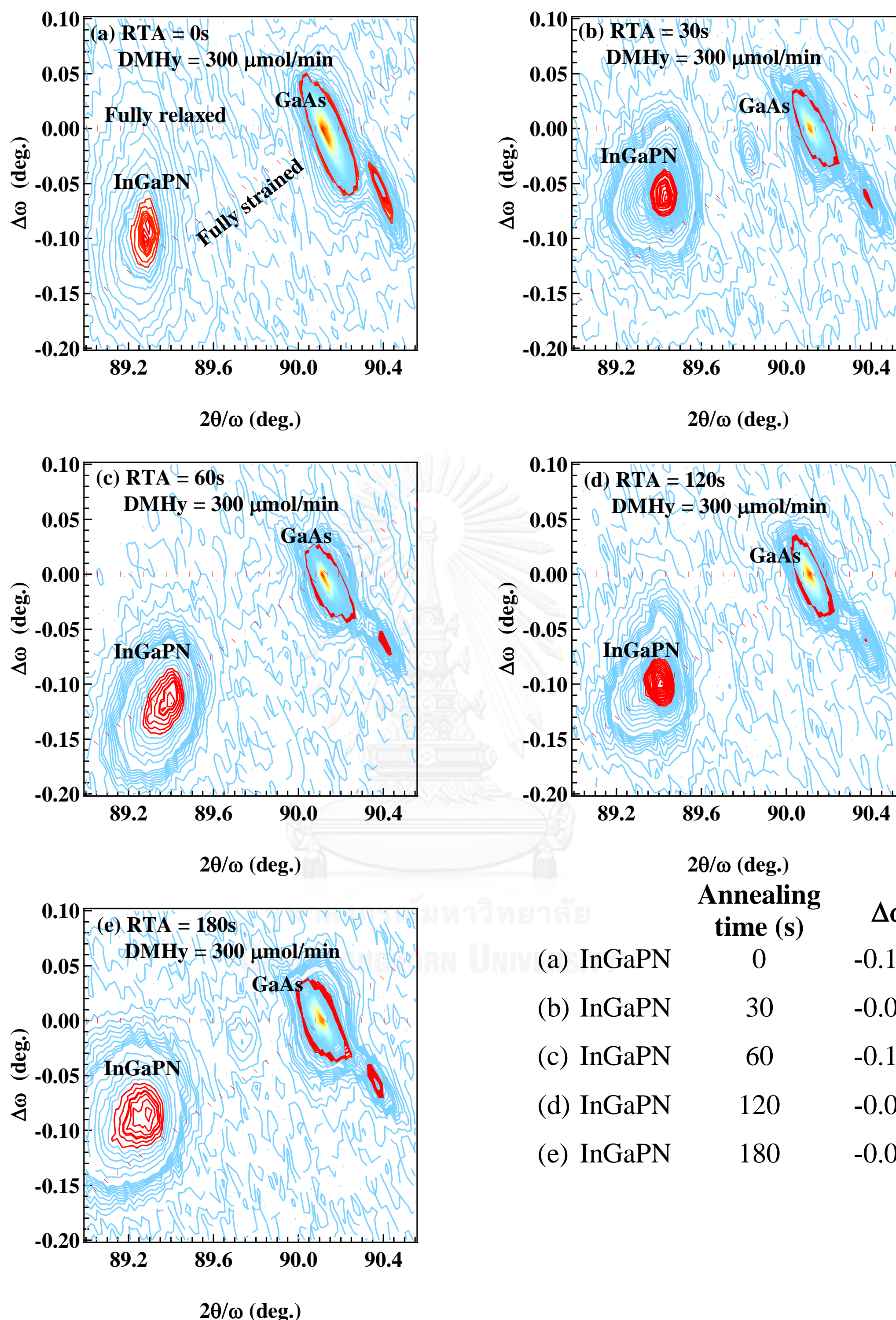

	Annealing time (s)	Δω
(a) InGaPN	0	-0.103
(b) InGaPN	30	-0.064
(c) InGaPN	60	-0.118
(d) InGaPN	120	-0.090
(e) InGaPN	180	-0.077

Fig. 4-17 HRXRD 2θ/ω and Δω reciprocal space maps around an asymmetrical (115) reflection for the InGaPN films on GaAs (001) on the DMHy flow rates 300 µmol/min with annealing time (a) as grown, (b) 30, (c) 60, (d) 120 and (e) 180 s at 650 ^{O}C.

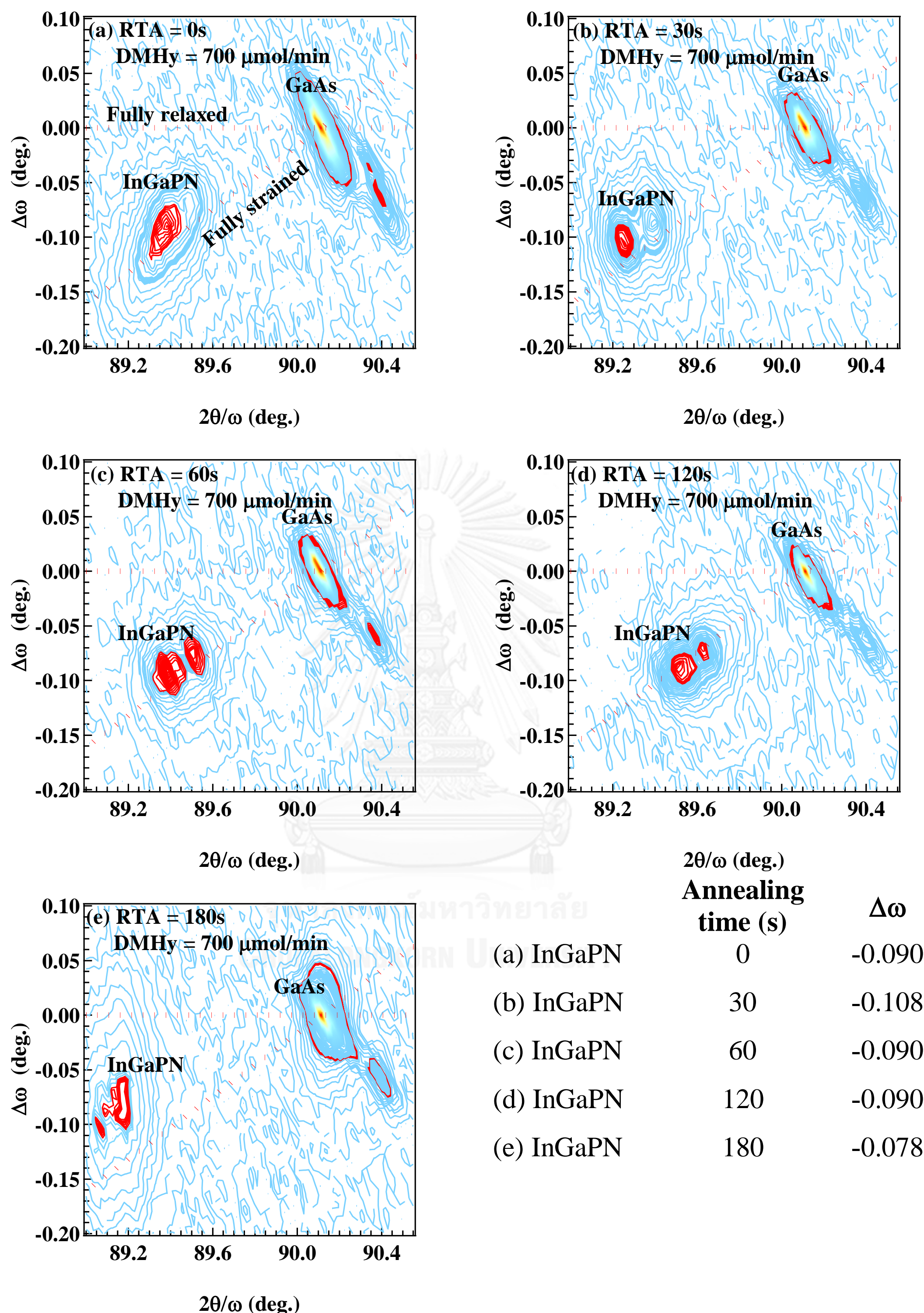

	Annealing time (s)	Δω
(a) InGaPN	0	-0.090
(b) InGaPN	30	-0.108
(c) InGaPN	60	-0.090
(d) InGaPN	120	-0.090
(e) InGaPN	180	-0.078

Fig. 4-18 HRXRD 2θ/ω and Δω reciprocal space maps around an asymmetrical (115) reflection for the InGaPN films on GaAs (001) on the DMHy flow rates 700 µmol/min with annealing time (a) as grown, (b) 30, (c) 60, (d) 120 and (e) 180 s at 650 ^{O}C.

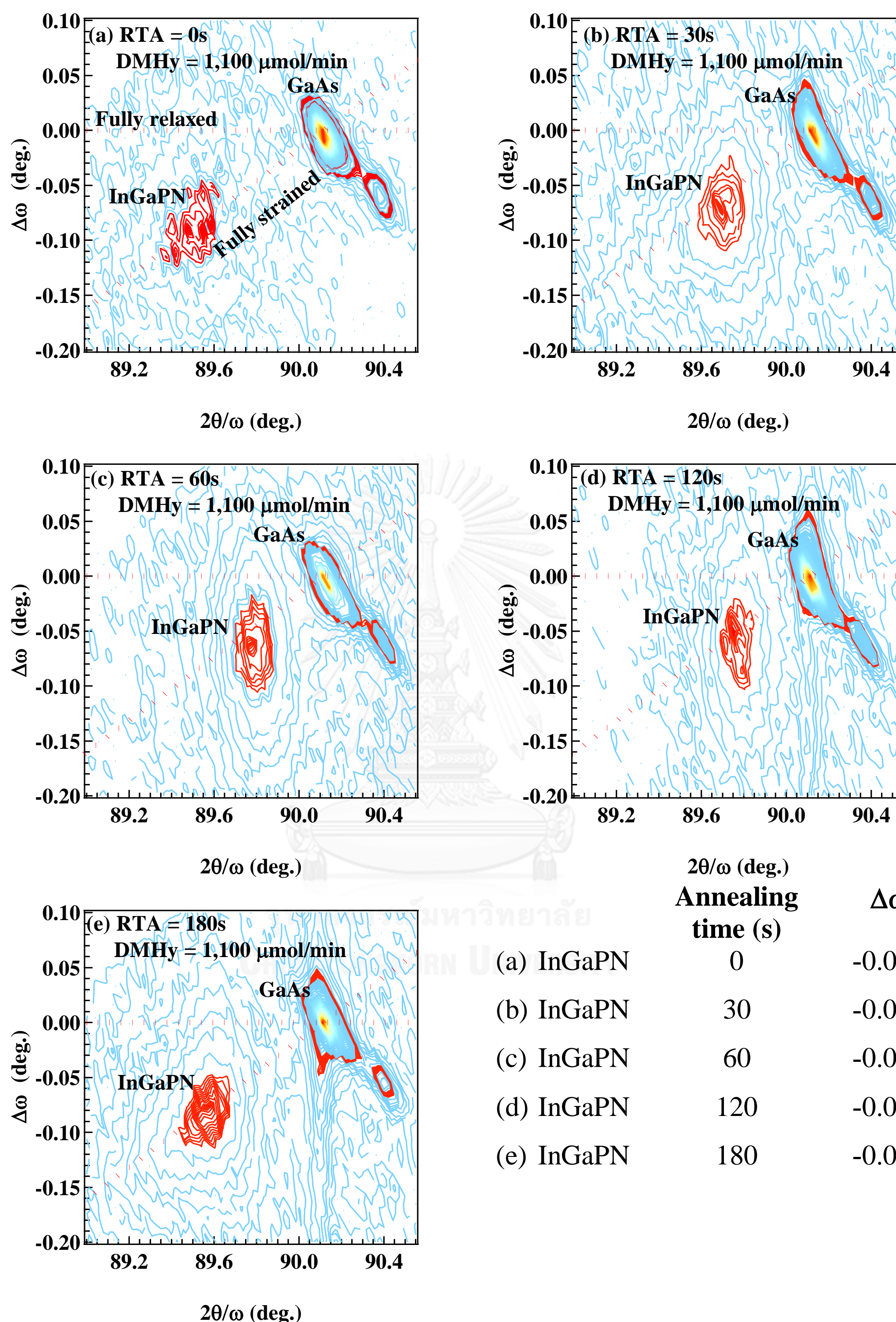

	Annealing time (s)	Δω
(a) InGaPN	0	-0.092
(b) InGaPN	30	-0.073
(c) InGaPN	60	-0.064
(d) InGaPN	120	-0.051
(e) InGaPN	180	-0.078

Fig. 4-19 HRXRD 2θ/ω and Δω reciprocal space maps around an asymmetrical (115) reflection for the InGaPN films on GaAs (001) on the DMHy flow rates 1,100 μmol/min with annealing time (a) as grown, (b) 30, (c) 60, (d) 120 and (e) 180 s at 650 ^{O}C.

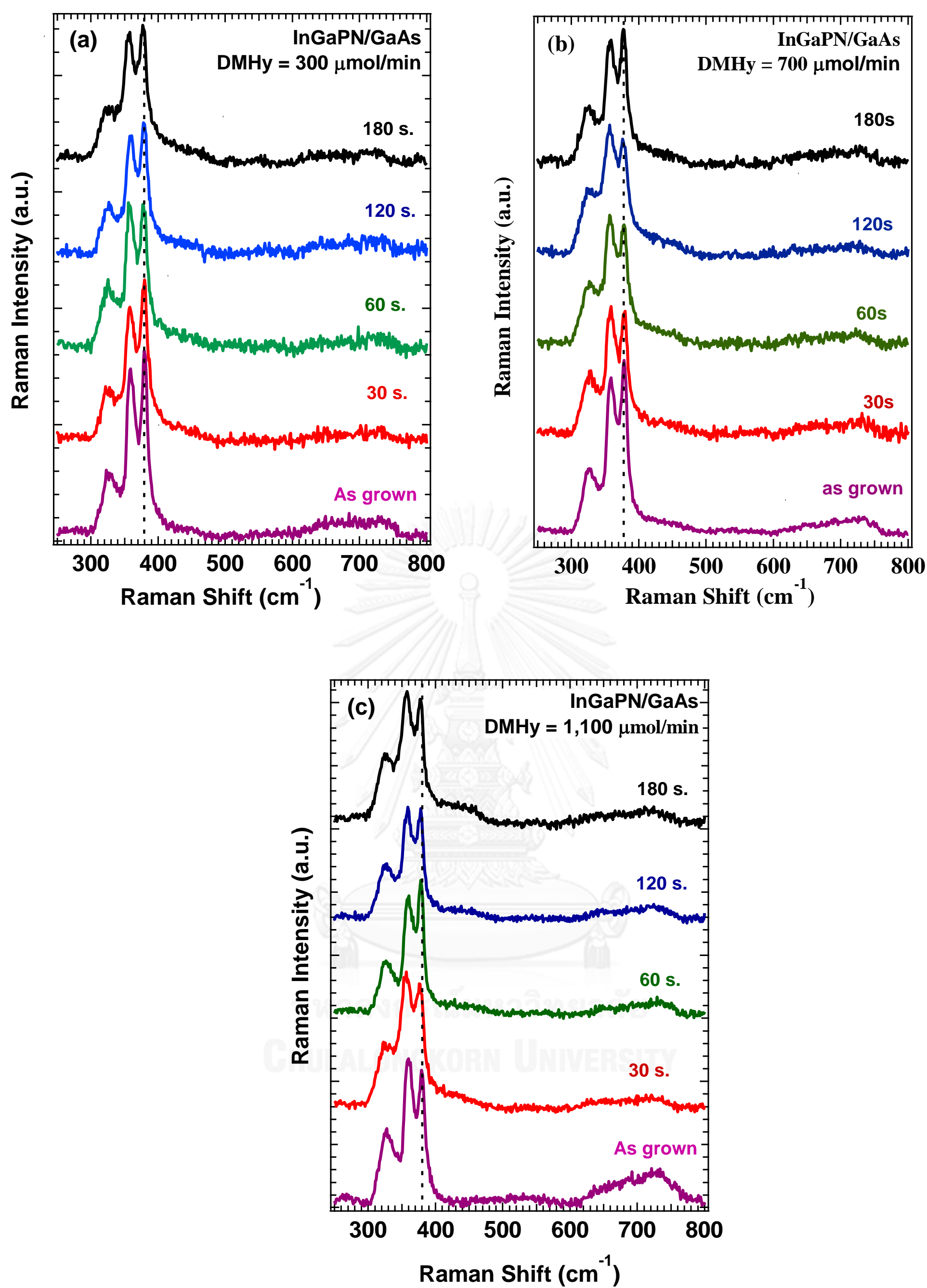

Fig. 4-20 illustrate Raman spectra of the InGaPN alloy films with different DMHy flow rates of (a) 300, (b) 700 and (c) 1,100 μmol/min, respectively. The different annealing time were applied to as grown and annealed InGaPN at 30, 60, 120, and 180 s. for each DHMy flow rates.

Table 4-4 Relaxed lattice constant (a_o), misfit strain ($\varepsilon_{||}$) and In content determined by micro-Raman spectroscopy) and calculated N content of DMHy 300 μmol/min.

Annealing Time (s)	GaP-LO (cm^{-1})	$a_\perp$ (Å)	$a_{\|}$ (Å)	a_o (Å)	Misfit strain(%)	In (%)	N (%)
As grown	378.7±0.5	5.70	5.66	5.68	0.47	55.8±0.8	0.9±0.4
30	378.4±0.5	5.69	5.67	5.68	0.41	56.2±0.8	0.9±0.4
60	377.2±0.6	5.70	5.65	5.68	0.39	58.2±0.9	2.0±0.4
120	377.2±0.6	5.69	5.65	5.67	0.33	58.2±1.1	2.4±0.4
180	377.0±0.6	5.70	5.67	5.68	0.54	58.5±1.1	1.2±0.4

Table 4-5 Relaxed lattice constant (a_o), misfit strain ($\varepsilon_{||}$) and In content determined by micro-Raman spectroscopy) and calculated N content of DMHy 700 μmol/min.

Annealing Time (s)	GaP-LO (cm^{-1})	$a_\perp$ (Å)	$a_{\|}$ (Å)	a_o (Å)	Misfit strain(%)	In (%)	N (%)
As grown	378.6±0.5	5.69	5.65	5.67	0.30	55.9±0.8	1.4±0.4
30	378.0±0.5	5.69	5.65	5.67	0.36	56.8±0.8	1.5±0.4
60	377.2±0.6	5.69	5.65	5.67	0.32	58.2±0.9	2.4±0.4
120	377.2±0.6	5.69	5.65	5.67	0.30	58.2±1.1	2.5±0.4
180	376.0±0.6	5.71	5.68	5.70	0.77	60.2±1.1	0.5±0.4

Table 4-6 Relaxed lattice constant (a_o), misfit strain ($\varepsilon_{||}$) and In content determined by micro-Raman spectroscopy) and calculated N content of DMHy 1,100 μmol/min.

Annealing Time (s)	GaP-LO (cm^{-1})	$a_\perp$ (Å)	$a_{\|}$ (Å)	a_o (Å)	Misfit strain(%)	In (%)	N (%)
As grown	378.7±0.5	5.67	5.65	5.66	0.12	55.7±0.8	2.1±0.4
30	377.8±0.5	5.68	5.65	5.67	0.25	57.2±0.8	2.4±0.4
60	377.6±0.6	5.68	5.65	5.67	0.22	57.5±0.9	2.7±0.4
120	377.6±0.6	5.67	5.66	5.66	0.20	57.5±1.1	2.8±0.4
180	377.2±0.6	5.68	5.65	5.67	0.26	58.2±1.1	1.7±0.4

Chulalongkorn University

When the annealing time increase from as grown sample up to 120s annealed samples, the diffraction contour of InGaPN (115) show the trend that moving align orientation along the full strained line (dash line as shown in Fig. 4-6, 4-7 and 4-8 (a) to GaAs (115)). This moving trend is similar occur like the increasing DMHy flow rate of the InGaPN which indicated that more N content are incorporate into the sample layers. However, at 180 s. of annealing time, the InGaPN (115) contour shifts back away from the fully strained line which cause the InGaPN layer are partial strained.

Fig. 4-20 show Raman spectra of the InGaPN alloy films with different DMHy flow rates of (a) 300, (b) 700 and (c) 1,100 μmol/min, respectively. The different annealing times were applied to as grown and annealed InGaPN at 30, 60, 120, and 180 s. for each DHMy flow rates. The similar spectrum of as grown and post-grown annealing can be observed. The GaP-like LO, InP-like LO and InP-like TO phonons are also observed for all the InGaPN films. The GaP-Like LO peak position of the annealed InGaPN show the slightly shift compare to as grown InGaPN resulting the change in In contents in InGaPN alloys. In addition, the InGaN related peak at around 730 cm^{-1} of the InGaPN show the slightly decrease trend compare to the as grown InGaPN. From the HRXRD and Raman results suggesting that the change of the alloy composition not only the N contents but also the In contents.

Then, to determine the alloy composition changed in InGaPN due to the duration time of annealing effect, the In content can be validate by Raman scattering and N content can determined by (004) $2\theta/\omega$ and (115) reciprocal mode. The alloy composition results are show in table 4-4, 4-5 and 4-6 for InGaPN with DMHy flow rate 300, 700 and 1,100 μmol/min, respectively. From the table 4-3, 4-4 and 4-5 results, the annealing effect cause the change in the alloy composition, both N and In content,

and also the strained changed in InGaPN. The strained show the reduced trend from as grown sample up to 120 s. annealed samples and dramatically increased at the 180 s. of annealing time.

From the alloy composition results, the post-growth rapid thermal annealing process show the significant impact to the structural properties of the InGaPN. The alloy composition, both In and N, are changed depend on the annealing time. This alloy composition changed leading to the change of the surface RMS and the misfit strained of the alloy film.

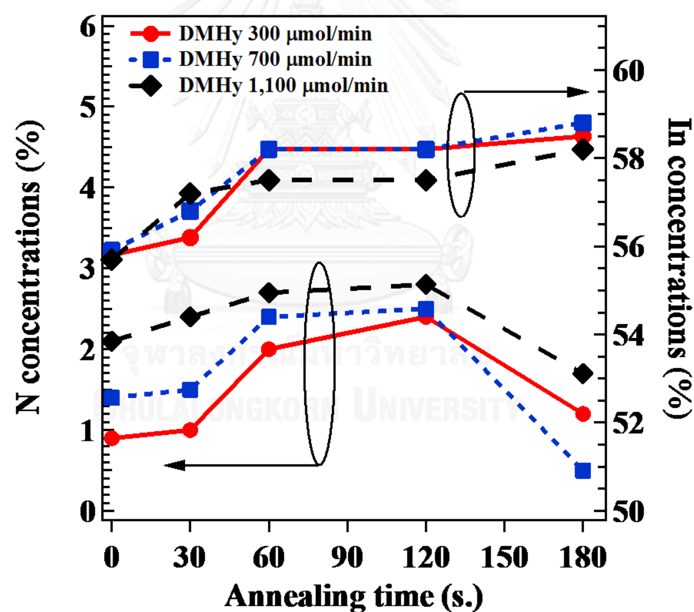

Fig. 4-21 In and N content as the function annealing time of (●) DMHy 300 μmol/min, (■) DMHy 700 μmol/min and (♦) 1,100 μmol/min.

4.3.3 Non-radiative Recombination Center after RTA

The post-growth RTA were applied to InGaPN to reduce non-radiative recombination center which reduced the PL intensity from the section 4.2.3. Fig. 4-23 show PL spectra of the InGaPN with different DMHy (a) 300, (b) 700 and (c) 1,100 μmol/min of as grown and annealed InGaPN at 30, 60, 120 and 180 s. of annealing time at 650 ^{O}C. The slightly blue-shifted of the annealing InGaPN band-gap energy can be observed from the as grown sample up to 120 s. annealing samples. This blue-shift occurs due to the higher amount of the N incorporation in InGaPN layer. The red-shifted occurs at 180 s. of annealing time for 300 and 700 μmol/min samples. The red-shifted are due to the reduced N incorporation in InGaPN. However, the red-shift of the band-gap energy can be observes at 180 s. 1,100 μmol/min that is related to the increasing of N incorporation in InGaPN as shown in table 4-7. The results of the shifted of the band-gap energy are agreed with the N contents changed in the alloy composition determined by HRXRD and Raman measurement. The intensity of the Pl spectra show an increase up to 120 s. of annealing time. The atoms gain the energy form the RTA can diffusion from the interstitial site to the lattice site cause an increasing of the PL intensity. Which indicated that the RTA process can reduced the non-radiative recombination and increase the luminescence in InGaPN. By the way, at 180 s. the decreasing of the intensity can be observe which due to exceed thermal energy at the longer time of an annealing can be damage the crystals which result in the reduction of the PL intensity. By the way, The FWHM of the PL spectra don’t change with and annealing time, which can interpreted that RTA process are less effect on the alloy fluctuation in InGaPN.

จุฬาลงกรณ์มหาวิทยาลัย
Chulalongkorn University

Table 4-7 show the band-gap energy of the annealing InGaPN with vary DMHy 300, 700 and 1,100 µmol/min

Annealing time (s)	DMHy 300 µmol/min	DMHy 700 µmol/min	DMHy 1,100 µmol/min
As grown	1.85	1.82	1.78
30	1.85	1.82	1.81
60	1.85	1.84	1.80
120	1.86	1.83	1.81
180	1.83	1.80	1.82

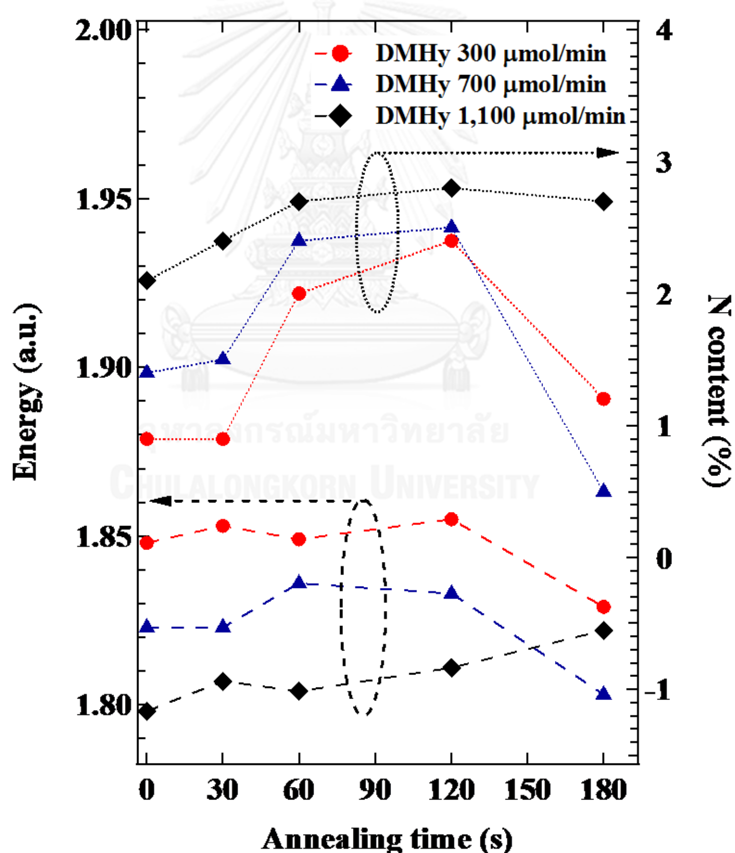

Fig. 4-22 a room-temperature PL of (a) annealing InGaPN with various DMHy flow rates and N contents as the function of the annealing times.

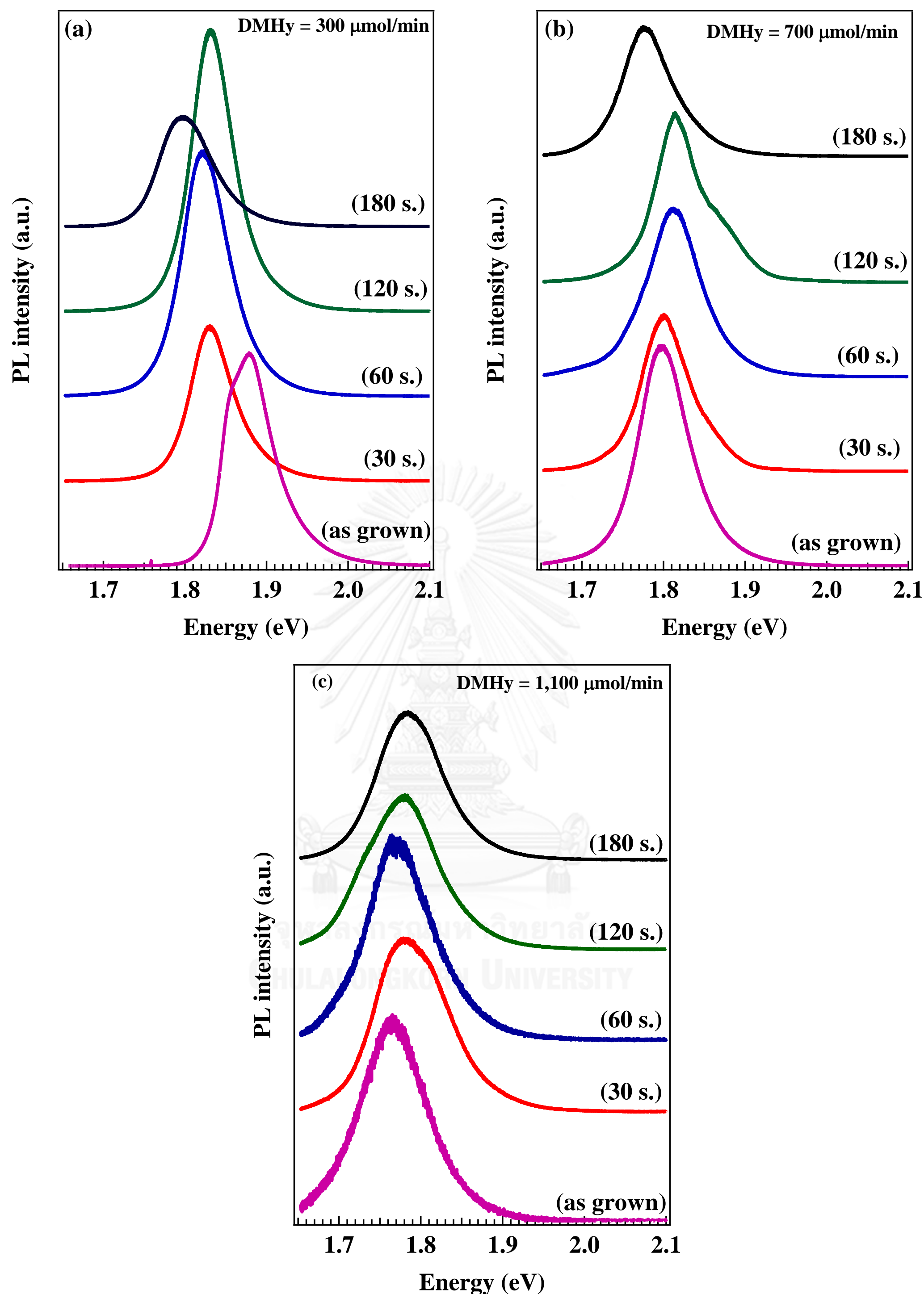

Fig. 4-23 a room-temperature PL of (a) annealing InGaPN with various DMHy flow rates (a) 300, (b) 700 and (c) 1,100 μmol/min. The annealing time is 0 (as grown), 30, 60, 120 and 180 s. as label in the graph.

4.3.4 Ordering Effect on N Contents after RTA

Due to the post growth annealing process cause the composition of InGaPN alloy changed. The b/a ratios are also show the change related to the N content in InGaPN as shown in Fig. 4-24. The b/a ratios are reduced (an increased order parameter, η) when the N content increasing from as grown InGaPN up to 120 s. and increased at 180 s. of annealing time. The increasing of b/a ration at 180 s. annealing times related to the decreasing of N contents. The b/a ratio reduced is implied to the more order of the ordering effect. The value of b/a ratio of the annealing InGaPN is in still in the same range compare to the as grown InGaPN which less than the distribution of the band-gap energy due to the random position. Then we can still conclude that the band-gap energy reduction are not effected from the ordering effect.

Table 4-8 show the b/a ratio of the annealing InGaPN with vary DMHy 300, 700 and 1,100 μmol/min

Annealing time (s)	DMHy 300 μmol/min	DMHy 700 μmol/min	DMHy 1,100 μmol/min
As grown	0.41	0.39	0.30
30	0.41	0.38	0.32
60	0.39	0.36	0.31
120	0.32	0.3	0.3
180	0.34	0.32	0.33

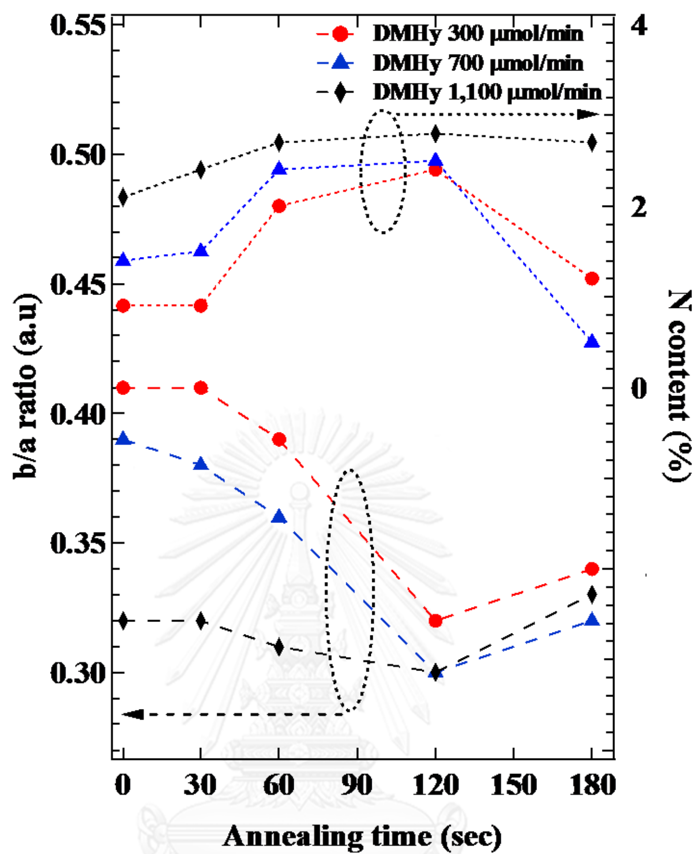

Fig. 4-24 show the b/a ratio and N content as the function of annealing time of InGaPN with different DMHy flow rate.

จุฬาลงกรณ์มหาวิทยาลัย
CHULALONGKORN UNIVERSITY

CHAPTER V
CONCLUSIONS

จุฬาลงกรณ์มหาวิทยาลัย
CHULALONGKORN UNIVERSITY

In this dissertation, the structural and optical properties of the as grown and annealing InGaPN on GaAs substrates are studied. The both as grown and annealing InGaPN samples which are studied in this work were grown and annealed by MOVPE method at Onabe Laboratory, University of Tokyo, Japan. The InGaPN samples were grown at different DMHy flow rates 0, 300, 700 and 1,100 μmol/min and annealed at 650 ^{O}C at 30, 60, 120 and 180 seconds by post growth annealing process. The structural and optical properties of as grown and annealing InGaPN are summarized as follows:

i) An adding N content cause increasing of In content and ordering

ii) A reduction of band-gap of InGaPN is found to resulting from the competition of alloying effect and ordering effect. In our case, the weak ordering was observed to be the level that no effect on optical bandgap.

iii) The post growth annealing process can be used to improve the alloy uniformity and reduce non-radiative recombination center of the InGaPN by selecting the best annealing.

iv) A combination of High Resolution X-ray diffraction (HRXRD) and Raman spectroscopy is an alternative method to find the alloy compositions in the quaternary InGaPN alloys.

v) An incorporation of N significantly influenced on a misfit strain in the InGaPN films. We achieved a nearly lattice-matched InGaPN film to GaAs with the lowest magnitude of misfit strain of 0.12%.

From our result, the nearly latticed-matched InGaPN on GaAs (001) substrate can achieve by using LP-MOVPE with a lowest misfit strained at 0.12%. The optimized annealing time used to improve the alloy uniformity and reduce non-radiative recombination center of the InGaPN

จุฬาลงกรณ์มหาวิทยาลัย
Chulalongkorn University

Future work

Form our results we would like to study on the electrical properties of Si-doped InGaPN films which grown with varying Si-precursor flow. The electrical properties of InGaPN layers grown lattice matched on GaAs substrate exhibited a back-ground p-type contamination of the order of 10^{16} cm^{-3}. With a Si-dope, the n-type of InGaPN are evidence with the number of free electron carrier is increasing from 3.6×10^{16} to 6×10^{18} cm^{-3} depending on Si precursor flow. When increase the N content in $In_xGa_{1-x}P_{1-y}N_y$, y>> 0.005, the band off set of the conduction band will be dramatically falls which the band alignment switch from the type-I quantum well to type-II quantum well. The energy band diagram of InGaPN/GaAs type-II quantum well which the band structure showed the separating electron and holes path without a complicated design of the P-N junction structure. From these steps, the natural PN-junction can be achieve with growth Si-doped InGaPN and un-dope InGaPN on GaAs substrate then the electrical properties will be studied which can lead us to achieve a high efficiency solar cells.

Chulalongkorn University

REFERENCES

1. D. Kaewket, S.S., S. Tungasmita, R. Katayama and K. Onabe, *MOVPE growth of high optical quality InGaPN layers on GaAs (001) substrates.* Phys. Status Solidi C, 2010. **7**: p. 2079-2081.
2. Y. G. Hong, R.A.a.C.W.T., *Gas-source molecular beam expitaxy of GaInNP/GaAs and a study of its band lineup.* J. Vac. Sci. Technol, 2001. **B19**: p. 1413.
3. D. Kaewket, S.T., S. Sanorpim, R. Katayama and K. Onabe, *InGaPN/GaP Lattice-Matched Single Quantum Wells on GaP (001) Grown by MOVPE.* Adv. Mater. Res, 2008. **55**: p. 821-824.
4. C. W. Tu, W.M.C., I. A. Buyanova and J. S. Hwang, *Material properties of dilute nitrides: Ga(In)NAs and Ga(In)NP.* J. Cryst. Growth, 2006. **288**: p. 7-11.
5. H. P. Xin, R.J.W., Y. G. Hong and C. W. Tu, *Gas-source MBE growth of Ga(In)NP/GaP structures and their applications for red light-emitting diode.* J. Cryst. Growth, 2001. **227**: p. 558-561.
6. Tu, V.A.O.a.C.W., *Growth and fabrication of InGaNP-based yellow-red light emitting diodes.* Appl. Phys. Lett, 2006. **89**: p. 191.
7. W. Guter, J.S., S.P. Philipps, M. Steiner, G. Siefer, A. Wekkeli, E. Welser, E. Oliva, A.W. Bett, F. Dimroth, *Current-matched triple-junction solar cell reaching 41.1% conversion efficiency under concentrated sunlight* Appl. Phys. Lett., 2009. **94**: p. 223504.
8. M. Yamaguchi, K.N., T. Sasaki, H. Suzuki, K. Arafune, N. Kojima, Y. Ohsita, Y. Okada, A. Yamamoto, T. Takamoto, K. Araki, *Novel materials for high-energy III-V multi-junction solar cells.* Solar Energy 2008. **82**: p. 173-180.
9. K. I. Lin, T.S.W., Y. T. Lu, and J. S. Hwang, *Valence-band splitting in InGaPN: Effects of epitaxial strain and atomic ordering* J. Appl. Phys, 2006. **99**: p. 056103.
10. H. Asahi, S.E., S. Gonda, Y. Kawamura, H. Tanaka, *Raman scattering in InGaAlP layers grown by molecular-beam epitaxy* J. Appl. Phys, 1989. **65**: p. 5007.
11. S. F. Yoon, K.W.M., H.Q. Zheng, B.P. Gay and P.H. Zhang, *Observation of weak ordering effects and surface morphology study of InGaP grown by solid source molecular beam epitaxy.* Microelectronics Journal 2000. **31**: p. 15-21.
12. S. Neumann, P.V., J. Spieler, T. Kippenberg, A. Lese, *LP-MOVPE Growth and Characterization of order InxGa1-xAsyP1-y using Non-Gaseous source in N2-carrier gas* Solid-State Electronics, 2000: p. 15-18.
13. M.C. Delong, D.J.M., R. A. Hogg, M. S. Skolnick, *Photoluminescence, photoluminescence excitation, and resonant Raman spectroscopy of disordered and ordered Ga0.52In0.48P* J.Appl. Phys, 1993. **73**(10): p. 5163.
14. N. V. Besslov, T.T.D., A. N. Efimov, N. F. Kartenko and YuP. Yakovlev, Sov. Phys. Solid State (English Transl.), , 1982. **22**: p. 1652.
15. D. D. Sell, H.C.C.a.K.W.W., *Concentration dependence of the refractive index for n - and p -type GaAs between 1.2 and 1.8 eV.* J. Appl. Phys, 1974. **45**: p. 2650.

จุฬาลงกรณ์มหาวิทยาลัย
Chulalongkorn University

16. G. Giesecke, H.P., *Präzisionsbestimmung der Gitterkonstanten von AIIIBv-Verbindungen, Präzisionsbestimmung der Gitterkonstanten von AIIIBv-Verbindungen.* Acta Crystallogr, 1958. **11**: p. 369.
17. M. Bugajski, W.J.L., *Concentration-dependent absorption and photoluminescence of n-type InP.* J. Appl. Phys, 1985. **57**: p. 521.
18. Gayton, F.S.H.a.W.R., *Elastic Constants of Single-Crystal Indium Phosphide.* J. Appl. Phys, 1966. **37**: p. 462.
19. Drummond, M.E.S.a.T.J., *Predicted elastic constants and critical layer thicknesses for cubic phase AlN, GaN, and InN on β-SiC.* J. Appl. Phys, 1991. **69**: p. 8423.
20. I. Vurgaftman, J.R.M.a.L.R.R.-M., *Band parameters for III–V compound semiconductors and their alloys.* J. Appl. Phys, 2011. **89**.
21. Queisser, W.S.a.H.j., *Detailed balance limit of efficiency of p-n junction solar cells.* J. Appl Phys, 1961. **32**: p. 510-519.
22. A. W. Bett, F.D.a.G.S., *Multijunction concentrator solar cells.* Concentrator photovoltaics, 2007: p. 67-87.
23. A. Hassine, J.S., P.L. Berre, M.A. Poission, F. Alexandre, M. Quillec, *Supperlattice effects induced by atomic ordering on GaxIn12xP.* Phys. Rev. B 1996. **54**: p. 2728-2733.
24. T. S. Wang, K.I.L.a.J.S.H., *Characteristics of InGaPN/GaAs heterostructures investigated by photoreflectance spectroscopy.* J. Appl. Phys, 2006. **100**: p. 093709.
25. K. I. Lin, J.Y.L., T. S. Wang, S. H. Hsu, J. S. Hwang, Y. G. Hong and C. W. Tu, *Effects of weak ordering of InGaPN.* Appl. Phys Lett, 2005. **86**: p. 211914.
26. D. Kaewket, S.S., S. Tungasmita, R. Katayama and K. Onabe, *Band alignment of lattice-matched InGaPN/GaAs and GaAs/InGaPN quantum wells grown by MOVPE.* Physica E, 2010. **42**: p. 1176-1179.
27. E. Bedel, R.C., G. Landa, and J. B. Renucci, *Selectivity of resonant Raman scattering in InAsxP1−x solid solutions.* Rev. Phys. Appl, 1984. **30**: p. 5923.
28. K. M. Kim, S.N., D. Krishnamurthy, S. Emura, S. Hasegawa and H. Asahi, *Optical properties of InGaPN epilayer with low nitrogen content grown by molecular beam epitaxy.* Journal of applied physics 2012. **112**: p. 063507.
29. S. Sakai, Y.U., Y. Terauchi, *Band gap energy and band lineup of III-V alloy semiconductors incorporating nitrogen and boron.* Jpn J. Appl. Phys, 1993. **32**: p. 4413.
30. L. Bellaiche, S.H.W.a.A.Z., *Band gaps of GaPN and GaAsN alloys.* Appl. Phys. Lett, 1997. **70**(26): p. 3558.
31. T. Makimoto, H.S., T. Nishida and N. Kobayashi, *Excitonic luminescence and absorption in dilute GaAs1 - xNx alloy (x < 0.3%).* Appl. Phys. Letts, 1997. **70**(22): p. 2984.
32. Tu, W.G.B.a.C.W., *Bowing parameter of the band-gap energy of GaNxAs1−x.* Appl. Phys. Lett, 1997. **70**(2): p. 1608.
33. S. Sakuntam, F.N., N. Nakadan, T. Kimura, R. Katayama, K. Onabe, *Growth and post-growth rapid thermal annealing of InGaPN on GaP grown by metalorganic vapor phase epitaxy.* Journal of Crystal Growth 2007. **298**: p. 150-153.

APPENDIX

จุฬาลงกรณ์มหาวิทยาลัย
Chulalongkorn University

APPENDIX A

LIST OF PUBLICATION AND CONFERENCE

PUBLICATION:

1) **Sritonwong, P.,** Sanorpim, S. and Onabe, K., Composition Investigations of Nearly Lattice-Matched InGaPN Films on GaAs (001) Substrates Grown by MOVPE. Chiang Mai Journal of Science. 2016; 43(2) : 288-295

CONFERENCES:

1) **Sritonwong, P.,** Sanorpim, S. and Onabe, K., Structural and optical properties of InGaPN/GaAs(001), The Science Forum 2011, Bangkok, Thailand, March 10-11, 2011. **(Oral presentation)**
2) **Sritonwong, P.,** Sanorpim, S. and Onabe, K., INVESTIGATION OF BAND GAP MODIFICATION IN LATTICED MATCHED InGaPN/GaAs (001) WITH INCORPORATION OF NITROGEN. Congress on science and technology of Thailand 39th (STT 39) : 2013 : Bangkok, Thailand, October 21-23, 2013. **(Poster presentation)**
3) **Sritonwong, P.,** Sanorpim, S. and Onabe, K., BANDGAP MODIFICATION IN LATTICED MATCHED InGaPN/GaAs (001) WITH INCORPORATION OF NITROGEN. The 9th Annual Conference of the Thai Physics Society Siam Physics Congress 2014: SPC2014, Nakorn Ratchasima, Thailand, March 26-29, 2014. **(Poster presentation)**

จุฬาลงกรณ์มหาวิทยาลัย
CHULALONGKORN UNIVERSITY

4) **Sritonwong, P.,** Sanorpim, S. and Onabe, K., Structural and Optical Investigations of Nearly Lattice-Matched InGaPN on GaAs (001) grown by MOVPE. 17th International Conference on Metalorganic Vapor Phase Epitaxy (ICMOVPE XVII), Lausanne, Switzerland, July 13-18, 2014. **(Poster presentation)**

5) **Sritonwong, P.,** Sanorpim, S. and Onabe, K., Structural and Optical Investigations of Nearly Lattice-Matched InGaPN on GaAs (001) grown by MOVPE. Workshop – Nanoscience & Nanomedicine, Nanyang Tehnological University, Singapore, September 11-12, 2014. **(Poster presentation)**

6) **Sritonwong, P.,** Sanorpim, S. and Onabe, K., Rapid thermal annealing and structural properties of lattice-matched InGaPN on GaAs (001) grown by MOVPE. The 10th Annual Conference of the Thai Physics Society Siam Physics Congress 2015: SPC2015, Krabi, Thailand, May 20-22, 2015. **(Oral presentation)**

จุฬาลงกรณ์มหาวิทยาลัย
Chulalongkorn University

VITA

Mr. Phongbandhu Sritonwong was born on August 14, 1982 in Nongkhai, Thailand. He received his bachelor degree of science in Physics from Chulalongkorn University in 2005 and master degree in Material Science and Nanotechnology from Linköping University, Sweden in 2007. He starts his work at Rajabhat Undornthani University and continues Doctor of Philosophy in Nanoscience and Technology, Graduate school of Chulalongkorn University in 2011.

During study PhD degree, he received financial support from Graduate school, Chulalongkorn University, Rajabhat Undornthani University, The Ratchadapiseksomphot Endowment Fund of Chulalonkorn University (RES560530229-EN) and The 90th Anniversary of Chulalongkorn University Fund (Ratchadapiseksomphot Endowment Fund).

While his studying in his PhD degree, he publishes the 1st international scientific paper in special issue 1 Chaing Mai Journal of science and got

1) The Second Prize Oral Presentation Award: Siam Physics Congress 2015, Sofitel Krabi Phokeethra Golf and Spa Resort, Krabi, Thailand on 20-22 May 2015

จุฬาลงกรณ์มหาวิทยาลัย
Chulalongkorn University

2) The Winner Prize in Material Student Competition: The 10th International Conference on the Physical Properties and Application of Advance Materials 2015, ICPMAT 2015, Chaing Mai, Thailand on 17-21 November 2015